Geographisches Institut
Eberhard Karls Universität Tübingen

Alfred-Wegener-Institut Potsdam
Helmholtz Zentrum für Polar- und Meeresforschung

Distribution and origin of organic matter in marine surface sediments on the Canadian Beaufort Shelf

Master thesis

to attain the academic degree
Master of Science (M.Sc.) in Physical Geography

submitted by

Katharina Schwarzkopf
4103330

First Reviewer: Dr. Peter Kühn
Second Reviewer: Dr. Michael Fritz

Tübingen, March 10, 2023

Katharina Schwarzkopf
born 21.05.1997 in Düsseldorf

Address:	Swetlana-Geier-Straße 36 79100 Freiburg
Student number:	4103330
Email:	katharina.schwarzkopf@student.uni-tuebingen.de

First Reviewer:	**Dr. Peter Kühn** **Eberhard Karls University of Tübingen** Soil Science and Geomorphology Rümelinstraße 19-23 72070 Tübingen
Email:	peter.kuehn@uni-tuebingen.de

Second Reviewer:	**Dr. Michael Fritz** **Alfred Wegener Institute** Helmholtz-Center for Polar and Marine Research Telegrafenberg A45 14473 Potsdam
Email:	michael.fritz@awi.de

Table of Contents

List of Figures ..... **V**

List of Abbreviations and Units ..... **VI**

Abstract ..... **VII**

Zusammenfassung ..... **VIII**

1. Introduction **1**

1.1. Knowledge Gaps 2

1.2. Study Aims and Objectives 3

1.3. Scientific Background 3

1.3.1. Sea Ice 3

1.3.2. Hydrography 4

1.3.3. Permafrost Coastal Erosion 4

1.3.4. Sediments 6

2. Study Area **7**

3. Material and Methods **9**

3.1. PeCaBeau 2021 Expedition and Sample Collection 9

3.2. Laboratory Analysis 11

3.2.1. Sample Preparation for Sediment Analysis 11

3.2.2. Grain Size Determination 13

3.2.3. Elemental Determination TOC, $\delta^{13}C_{org}$ / TN, $\delta^{15}N_{tot}$ / Mercury 13

3.2.4. ^{14}C-Dating 13

3.3. Data Evaluation/ Statistical Analysis 14

3.3.1. IDW-Interpolation 14

3.3.2. Spatial Analysis 15

3.3.3. Grain Size 15

3.3.4. TOC/TN/Hg/ Stable Isotopes 15

3.3.5. ^{14}C-Dating 16

4. Results **17**

4.1. Sediment Composition and Spatial Distribution 17

4.1.1. Grain Size 17

4.1.2. Total Organic Carbon 20
4.1.3. Total Nitrogen 21
4.1.4. C/N ratio 22
4.1.5. Mercury 23
4.1.6. $\Delta^{13}C_{org}$ 24
4.1.7. $\Delta^{15}N_{tot}$ 25
4.1.8. Bulk sediment age 26
4.2. Correlation Matrix 28
4.3. Dual-Carbon Isotope Endmember Modelling 31
5. Discussion 33
5.1. Origin of Organic Matter 33
5.2. Spatial Relationships and Distribution 36
5.3. Mobilization and Sedimentation of Mercury 40
5.4. Degradation of Organic Matter 41
6. Conclusion 43
7. References 45
Appendix 56
Acknowledgements 60
Declaration of Authorship 61

List of Figures

Fig. 1: Bathymetric Map of the Canadian Beaufort Sea 7

Fig. 2: Bathymetry 3D Modell 8

Fig. 3: Map of the study area with cruise track.....9

Fig. 4: Multicorer from AWI Bremerhaven on deck the CCGS Amundsen before deployment 10

Fig. 5: Schematic of multicorer sampling the seafloor.....11

Fig. 6: Workflow and Sample Preparation.....12

Fig. 7: Volume Distribution of Grain Size 18

Fig. 8: Interpolated Distribution Map of Grain Size (D50).....19

Fig. 9: Interpolated Distribution Map of Total Organic Carbon 20

Fig. 10: Interpolated Distribution Map of Total Nitrogen.....21

Fig. 11: Interpolated Distribution Map of C/N ratios 22

Fig. 12: Interpolated Distribution Map of Mercury 23

Fig. 13: Interpolated Distribution Map of $\delta^{13}C_{org}$.....24

Fig. 14: Interpolated Distribution Map of $\delta^{15}N_{tot}$.....25

Fig. 15: Interpolated Distribution Map of $\delta^{14}C$ 26

Fig. 16: Percentage Deviation between samples in 0-1 and 1-2 cm depth.....27

Fig. 17: Correlation Matrix 30

Fig. 18: Dual-Carbon Isotope Endmember Modelling 32

Fig. 19: Stable Isotope Endmember Modelling 34

Fig. 20: Map of the Canadian Beaufort Shelf with Influencing Currents 38

List of Abbreviations and Units

°C	Degree Celsius
BP	Before Present
cm	Centimeter
E	East
g	Gram
h	Hour
kg	Kilogram
km	Kilometer
m	Meter
mm	Millimeter
Mt	Megatons
m/a	Meter per Year
N	North
NOAA	National Oceanic and Atmospheric Administration
NSIDC	National Snow an Ice Data Center
S	South
s	Seconds
t	Ton
t/yr	Ton per Year
W	West
yr	Year
µg	Microgram
µm	Micrometer

Abstract

The Arctic Ocean's continental shelves are undergoing changes due to the effects of climate warming. As a result of increasing river discharge, deeper permafrost thaw, and coastal erosion, large amount of previously frozen carbon, nutrients and contaminants are being released into the nearshore zone. However, the interactions between these factors, the impact of external influences, and the fate of terrestrial organic matter are still unclear. This study aims to investigate the source and deposition patterns of organic matter in the Canadian Beaufort Sea. In fall of 2021, short cores were taken from 25 position along five transect that covered the Beaufort Sea Shelf. The upper two centimeters of the marine sediments were analyzed for organic carbon, nitrogen, mercury, and grain size. In addition, bulk ^{14}C radiocarbon ages and stable isotope ratios ($\delta^{13}C_{org}$ and $\delta^{15}N_{tot}$) were used to help distinguish sources and degradation status of terrestrial organic matter. Results show that the material is predominantly fine-grained clayey silt, and the bulk surface ages vary between 5500 and 10000 years before present. There are specific spatial distribution patterns of carbon and nitrogen, which highlight the influence of bathymetry, currents, and distance to the Mackenzie River delta on transport and degradation mechanisms of organic matter. Stable isotope composition shows a clear signature of terrestrial material on the shelf, whereas burial efficiency decreased with increasing distance from shore. Additionally, mercury distribution, influenced by grain size, organic matter content, and water depth, reveals the Canada basin acting as a sink for mercury. To conclude, this study shows the deposition patterns of organic matter and highlights the interactions of multiple external factors in understanding the fate of previously frozen carbon and contaminants in the Beaufort Sea.

Keywords: Arctic Ocean, Mackenzie River, permafrost thaw, coastal erosion, spatial distribution

Zusammenfassung

Die Kontinentalschelfe des Arktischen Ozeans verändern sich durch die Auswirkungen der Klimaerwärmung. Infolge des zunehmenden Abflusses von Flüssen, des Auftauens von Permafrostböden und der Küstenerosion werden große Mengen von zuvor gefrorenem Kohlenstoff, Nährstoffen und Schadstoffen in die küstennahe Zone freigesetzt. Die Wechselwirkungen zwischen diesen Faktoren, die Auswirkungen äußerer Einflüsse und der Verbleib des terrestrischen, organischen Materials sind jedoch noch unklar. Ziel dieser Studie ist es, die Quellen und Ablagerungsmuster organischer Stoffe in der kanadischen Beaufortsee zu untersuchen. Im Herbst 2021 wurden an 25 Stationen entlang von fünf Transekten, die den Schelf der Beaufortsee abdecken, kurze Bohrkerne entnommen. Die oberen zwei Zentimeter der Meeressedimente wurden auf organischen Kohlenstoff, Stickstoff, Quecksilber und Korngröße untersucht. Darüber hinaus wurden ^{14}C-Radiokohlenstoff-Alter und stabile Isotopenverhältnisse ($\delta^{13}C_{org}$ und $\delta^{15}N_{tot}$) verwendet, um die Quellen und den Abbaustatus des terrestrischen organischen Materials zu bestimmen. Die Ergebnisse zeigen, dass es sich bei dem Material überwiegend um feinkörnigen lehmigen Schluff handelt, und das Alter der Oberfläche variiert zwischen 5500 und 10000 Jahren vor der Gegenwart. Es gibt spezifische räumliche Verteilungsmuster von Kohlenstoff und Stickstoff, die den Einfluss der Bathymetrie, der Strömungen und der Entfernung zum Delta des Mackenzie River auf den Transport und die Abbauprozesse der organischen Substanz verdeutlichen. Die Zusammensetzung der stabilen Isotope zeigt ein deutliches Anzeichen von terrestrischem Material auf dem Schelf, während die Vergrabungseffizienz mit zunehmender Entfernung von der Küste abnimmt. Die Quecksilberverteilung, die von der Korngröße, dem Gehalt an organischem Material und der Wassertiefe abhängt, zeigt außerdem, dass das Kanada-Becken als Quecksilbersenke fungiert. Zusammenfassend lässt sich sagen, dass diese Studie die Ablagerungsmuster von organischem Material aufzeigt und die Wechselwirkungen mehrerer externer Faktoren beim Verständnis des Verbleibs von zuvor gefrorenem Kohlenstoff und Schadstoffen in der Beaufortsee verdeutlicht.

1. Introduction

As the Arctic experiences more rapid and significant changes in climate than any other region on Earth, permafrost soils of the Northern Hemisphere are becoming increasingly vulnerable to thawing (Schuur et al. 2015; Strauss et al. 2017). According to climate models, temperatures in the Arctic are projected to increase more rapidly than the global average, with surface temperatures expected to rise between 1°C (RCP 2.6) and 8°C (RCP 8.5) by the end of the 21st century (IPCC 2022). As permafrost thaws, organic matter (OM) that has previously been preserved by frozen ground conditions now becomes subject to microbial degradation with rising ground temperatures, resulting in the production of greenhouse gases (Tanski et al. 2021). This permafrost carbon feedback contributes to further global warming (Elberling et al. 2013; Knoblauch et al. 2013) and is highly debated as a global climate tipping point (Hollesen et al. 2015). At the same time, the Arctic Ocean is highly susceptible to the accumulation of mercury (Hg) due to long-range atmospheric transport of natural sources and anthropogenic emissions from lower latitudes (Driscoll et al. 2013; Schuur et al. 2015).

Continental margins, including deltas and shelves, are the primary sites of OM preservation in the ocean, accounting for over 80 % of global carbon burial (Hedges and Keil 1995). In the Canadian Beaufort Sea, erosion of unconsolidated permafrost soils results in the release of 4.9-14 megatons (Mt) of particulate organic carbon (POC) into the nearshore zone (Wegner et al. 2015). This represents more than four times the amount of POC contributed by major Arctic rivers (McClelland et al. 2016), highlighting the significant role that coastal erosion plays in the marine carbon budget of the Canadian Beaufort Sea. OM discharged by erosion can also have several other impacts: Besides being decomposed released as greenhouse gases, it can be redeposited on land or transported to aquatic systems where it can be further mineralized in the water column or buried in sediments (Letscher et al. 2011; Vonk et al. 2014; Fritz et al. 2017). The sedimentation of the Mackenzie river's material on the Beaufort Shelf provides a relevant source of OM to the seafloor (Rood et al. 2017). As the sediment accumulates, OM from terrestrial and marine sources is buried and preserved in the sedimentary record (Goñi et al. 2005). This carbon sequestration is an important process in the global carbon cycle. Furthermore, Hg contamination in the Canadian Arctic threatens the health of Arctic marine biota, as well as local inhabitants (Dietz et al. 2013). In the Canadian Arctic, contamination levels in wildlife remain high (Braune et al. 2015) and have increased in certain species (Castello et al. 2014). Riverine Hg export currently accounts for about 15-20 % of the Hg entering the

Arctic Ocean (Dastoor et al. 2022). This underscores the importance of addressing the sources of Hg pollution and distribution in Canada's Beaufort Sea, as it has implications for ecological health as well as for the livelihoods of local communities that depend on the region's natural resources. As climate change continues to affect the Arctic, the seaward transport of land-derived inorganic sediments and organic material is also expected to be changing drastically (Stern et al. 2012; Goñi et al. 2013).

Surface sediments on the seafloor contain valuable information about large-scale processes in the ocean, including OM supply, transport and degradation, bio productivity at the surface, and local geological settings (Coffin et al. 2017). One of the major challenges in understanding the biogeochemistry of the Arctic Ocean is determining the sources of organic carbon, which can either be autochthonous (primary production in overlying waters) or allochthonous (inputs from terrigenous sources) (Drenzek et al. 2007). Several studies have shown that data on OM composition can be used to differentiate between these two sources (Knies et al. 2007; Belicka and Harvey 2009; Yunker et al. 2011; Vonk et al. 2012; Goñi et al. 2013; Bröder et al. 2016).

1.1. Knowledge Gaps

Changes in Arctic river discharge (Doxaran et al. 2015), resuspension of sediments in nearshore waters (Fritz et al. 2017), permafrost coastal erosion (Schuur et al. 2015; Lantuit and Pollard 2008), and their impacts on Arctic coastal ecosystems have been the subject of several studies. The increasing rate of coastal erosion (Irrgang et al. 2018) and runoff from large river systems (Bring et al. 2016) is releasing higher amounts of OM into the nearshore zone, which is then transported to the Beaufort Shelf and possibly further offshore (Tanski et al. 2017). Several processes and factors such as currents, climatic factors and water depth are involved in the transport, distribution, and degradation of OM. However, little is known about how they interact with each other and affect the composition and fate of terrestrial and marine OM. Another process that is being amplified by climate change and permafrost thaw is the release of organic-bound Hg (Schuur et al. 2015). Permafrost soils represent a global Hg reservoir, although the fate of permafrost soil Hg after release is still unclear (Chételat et al. 2022).

1.2. Study Aims and Objectives

The Canadian Beaufort Sea is promising study region, given the high rates of coastal erosion and permafrost degradation (Couture et al. 2018), the high OM content (Goñi et al. 2005) in sediments and the large spatial scale, in which these various interacting processes can be investigated. By studying the sources, quantities and the lateral distribution of OM, this study aims to improve the understanding of the Canadian Beaufort Shelf as a carbon source or sink. Therefore, it contributes to filling the knowledge gap in understanding the carbon cycle and aspects of the Hg biogeochemical cycle in the Arctic. The overall aim of this study is to answer the question: What is the fate of OM in the Canadian Beaufort Sea? The specific objects are (1) to identify the sources of OM, (2) to understand how OM is transported and subsequently distributed spatially on the Beaufort Shelf, and (3) to improve the understanding of how the material is related to other environmental parameters such as water depth, currents, distance to the coast and/or the Mackenzie River Delta.

1.3. Scientific Background

1.3.1. Sea Ice

The southern Beaufort Sea represents one of the most ice-rich areas in the Canadian Arctic (Lantuit and Pollard 2008). It forms an interface between the atmosphere and the ocean and therefore influences surface moisture, heat and momentum fluxes (Meier et al. 2014). Ice formation is thermodynamic, but ice can also become thicker due to dynamic redistribution of the ice sheet caused by deformation and ice movement. The majority of the ice cover is affected in drift by wind, ocean currents, and density gradients at the sea surface (Meier et al. 2014). Arctic sea ice cover varies with season, reaching its maximum extent in late February/early March (5.05x106 km^2 in March 2020) (NSIDC, 2022). Throughout this period, it covers most of the Arctic Ocean and extends to the Sea of Okhotsk in the Pacific Ocean and Hudson Bay in the Atlantic Ocean (Meredith et al. 2019). As air temperature rises and when warm fresh water arrives in the Mackenzie Delta in mid-May, sea ice decreases and reaching its seasonal minimum in September (3.74x106 km^2 in September 2020) (NSIDC, 2022). However, it is not exceptional to find sea ice at the Canadian Beaufort Sea until mid-July (Doxaran et al. 2012). Due to climate change, ice extent has decreased in all months over the past 30 years, especially over the summer months. In September 2007, sea ice cover was 37 % lower than in the 1990s (Overland 2009). The ice cover is thinning and is increasingly dominated by younger, thinner ice types (Meier et al. 2014; Stroeve et al. 2014; Maslanik et al. 2011).

1.3.2. Hydrography

Many rivers of the northern Canadian coast flow into the Beaufort Sea and influence various geomorphological, hydrological and oceanographic processes. In particular, northern deltas represent biological hotspots to varying degrees (Lesack et al. 2013). The most crucial and largest river in this region is the Mackenzie River, forming a complex mosaic of over 45,000 lakes (Emmerton et al. 2007) along with a network of channels strongly influenced by ground ice and permafrost (Burn and Kokelj 2009). It is the longest river in Canada and enters the Canadian Beaufort Sea as a river delta west of Tuktoyaktuk. The Mackenzie Shelf has an area of $1.8x10^6$ km^2 and is seasonally ice covered (Osborne and Forest 2016). The freezing usually begins in mid-October. During the winter months, when immobile land fast ice covers the shelf (<20 m water depth), a two meter ice cover forms (Rachold et al. 2000). In late May/ early June the channels of the river thaw again. Thawing increases water discharge from about 150,000 m^3/s to 250,000 m^3/s (Lesack et al. 2013). The ice melt results in the release of freshwater containing sediment, and advection of runoff over the shelf and open water allows wave action (Osborne and Forest 2016). In summer, the marine surface circulation is mainly influenced by winds, the outflow of the Mackenzie River, and the anticyclonic Beaufort Gyre, which drives the nearshore currents westward, retaining most of the freshwater in the basin (Serreze et al. 2006; Mustapha et al. 2016). In terms of sea temperature, the Mackenzie Shelf is characterized by a strong temperature gradient: These are related to the wide extent of the Mackenzie River, leading to a decrease in surface water temperature (Mulligan et al. 2010). Overall, there is a strong variability in sea surface temperature, which is particularly influenced by winds (Mustapha et al. 2016).

1.3.3. Permafrost Coastal Erosion

Globally, 34 % of coasts are Arctic permafrost coasts and are therefore influenced by permafrost and seasonal sea ice cover (Lantuit et al. 2012). The entire Arctic Ocean coastline is 100,000 km long, of which one-third is classified as lithified and the remaining two-thirds consists of unconsolidated sediment (Lantuit et al. 2012). Due to the climatic conditions in the high latitudes, the sediments are deeply frozen. Permafrost has been defined as ground, which is frozen (>0°C) for at least two continuous years (Biskaborn et al. 2019). In the permafrost coastal system, permafrost occurs in the subaerial part of the coastal profile, as well as below the water column as submarine ground ice (Rachold et al. 2000). In summer, when air temperatures are well above freezing, the permafrost begins to thaw. Additionally, open water season exposes thawing coasts to erosion, which is influenced by thermoabrasion and thermodenudation (Günther et al. 2013). Further erosion forms

are: active layer detachment (Lewkowicz 1990), retrogressive thaw slumps (Lantuit and Pollard 2008), and block failure (Hoque and Pollard 2009). With the reduction in sea ice cover, wave energy increases, which also intensifies erosion (Lantuit and Pollard 2008). Consequently, the nearshore profile is deepened, and waves approach the coastline before breaking, resulting in increased breaking power (Dallimore et al. 1996). Erosion rates in arctic are in general higher than in other regions of the world, even though the process is limited to the summer months (Couture et al. 2018) and depend on various factors: cliff heights, ice content, orientation, annual air temp., length of the open water season, fetch length and wave energy (Lantuit and Pollard 2008). Intense storms, which are the primary cause of erosion in the Arctic, occur throughout the year (Irrgang et al. 2022). However, impacts are limited from fall to spring due to sea ice cover, thus coastal erosion is conditioned to the ice-free summer season (Atkinson 2005; Aré 1988). Sediment mobilized by coastal erosion is often organic rich as Permafrost soils store about 60 % (1,035 ± 150 Mt) of global soil carbon (Hugelius et al. 2014). As this carbon is frozen and therefore protected from biodegradation, it is prevented from the active carbon cycle. However, when permafrost thaws, carbon and other greenhouse gases like methane become bioavailable again, which will have a strong impact on the global climate system (Vonk et al. 2014; Biskaborn et al. 2019).

Nonetheless, not only will rising air temperatures lead to active layer deepening and permafrost thawing, but warmer seawater temperatures, sea level rise, and ice thinning will also influence warming and thus thawing of submarine permafrost in nearshore zones (IPCC 2022, Lantuit and Pollard 2008). Consequences of this is permafrost degradation, which is reflected in collapses of coastlines, causing release of large amounts of organic carbon in the nearshore zone (Fritz et al. 2017). In the last few decades, coastal erosion rates have more than doubled along many parts of the Beaufort Sea, amounting to a mean of 0.5 m per year (Lantuit et al. 2012). As a result, an estimated 14.0 Mt of particulate organic carbon is released annually in the nearshore zone (Wegner et al. 2015). Due to the ongoing climate change, coastal erosion rates accelerate with extreme average rates of more than 20 m/a (Jones et al. 2018). Since the transported material is not only rich in organic matter, but also contaminated by pollutants, an increase in sediment transport is considered to alter the ecosystem, as well as the global carbon cycle (Fritz et al. 2017).

1.3.4. Sediments

Terrestrial sediment input to the Canadian Beaufort Sea occurs from large rivers, like the Mackenzie River, eroding coastlines, and thawing permafrost (Osborne and Forest 2016). Sediments consist primarily of fine sands with minor clay and diamict (Rachold et al. 2000). The largest influence is the input from the Mackenzie River (Macdonald et al. 1998; Smith 2010). The river transports 125 million t/yr of mostly fine-grained material, of which a large portion is deposited in the delta and 50-70 % is deposited as sediment load on the inner shelf (Macdonald et al. 1998). About 20 % of the sediment is exported beyond the shelf edge (Osborne and Forest 2016). Approximately 1.5 million t/yr of terrestrial sediment load is derived from additional rivers flowing into the Canadian Beaufort Sea and 5.6 million t/yr is sourced from erosional decline of permafrost coasts (Hill et al. 1991). The organic carbon input from the permafrost coasts is fixed in the shelf sediments up to 12.7 %. The remaining fraction is either metabolized in the nearshore or transported off the shelf by wave action (Couture et al. 2018). The surface layer of the seafloor typically contains fine sands and silty clays, at a thickness of a few centimeters (Osborne and Forest 2016).

2. Study Area

The Beaufort Sea is a marginal sea of the Arctic Ocean located west of the Arctic Islands of Canada and north of the Northwest Territories and Yukon, Canada and Alaska. It covers an area of 476,000 km^2, with an average depth of 124 m (maximum depth is 4683 m). The study area is the Canadian Beaufort Shelf, which includes the Mackenzie Shelf and the Amundsen Gulf in the southeastern Beaufort Sea (Fig. 1). Surface water circulation is dominated by the wind-driven anticyclonic Beaufort Gyre, which drives nearshore currents westward and retains most of the Arctic Ocean freshwater in the Canada Basin (Serreze et al. 2006).

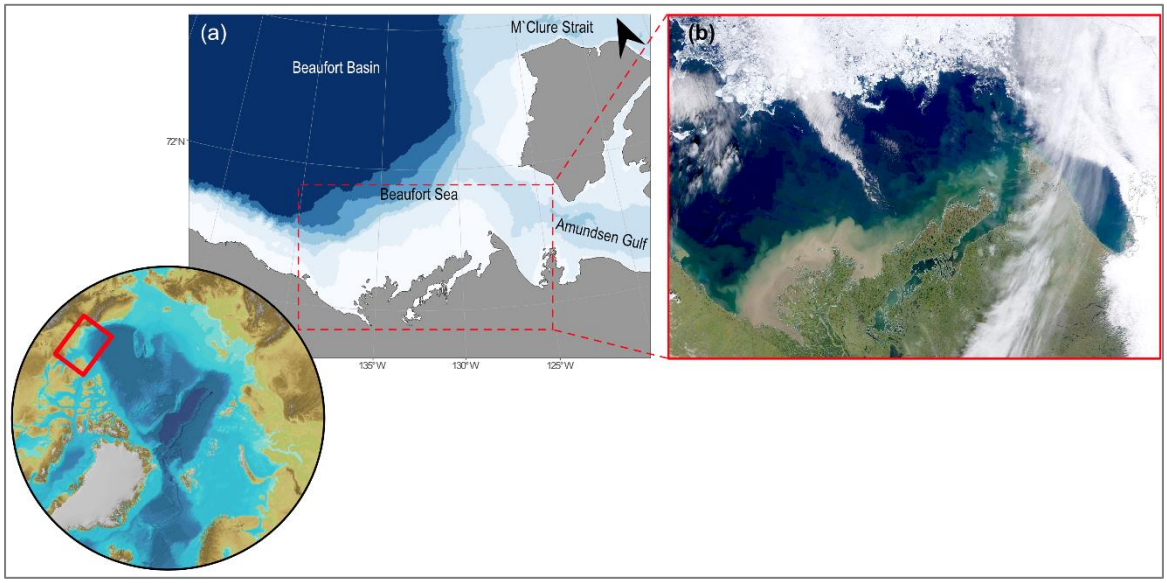

Fig. 1: (a) Bathymetric Map of the Canadian Beaufort Sea (source: ggOceanMaps), (b) The Mackenzie River plume on August 05, 2017 (source: EOSDIS Worldview Earth; https://worldview.earthdata.nasa.gov)

The Canadian Beaufort Shelf has a relief of approximately 80 m water depth, where the shelf break is located, transporting Pacific Water eastward along the slope (Nikolopoulos et al. 2009). Exceptions are the Mackenzie Trough, which is a glacial valley up to 300 m deep northeast of Herschel Island, and several smaller valleys (Carmack and Macdonald 2002). The bathymetry of the study is shown in a 3D model, with a clear visualization of the Mackenzie Trough and the shelf break (Fig. 2). During the Holocene, the seafloor was covered with about 30 m of sediment, consisting mainly of clay and silt (Richerol et al. 2008). The Mackenzie River supplies sediments and freshwater to the Canadian Beaufort Sea and drains an area of about 1,805,000 km^2 (Mulligan et al. 2010).

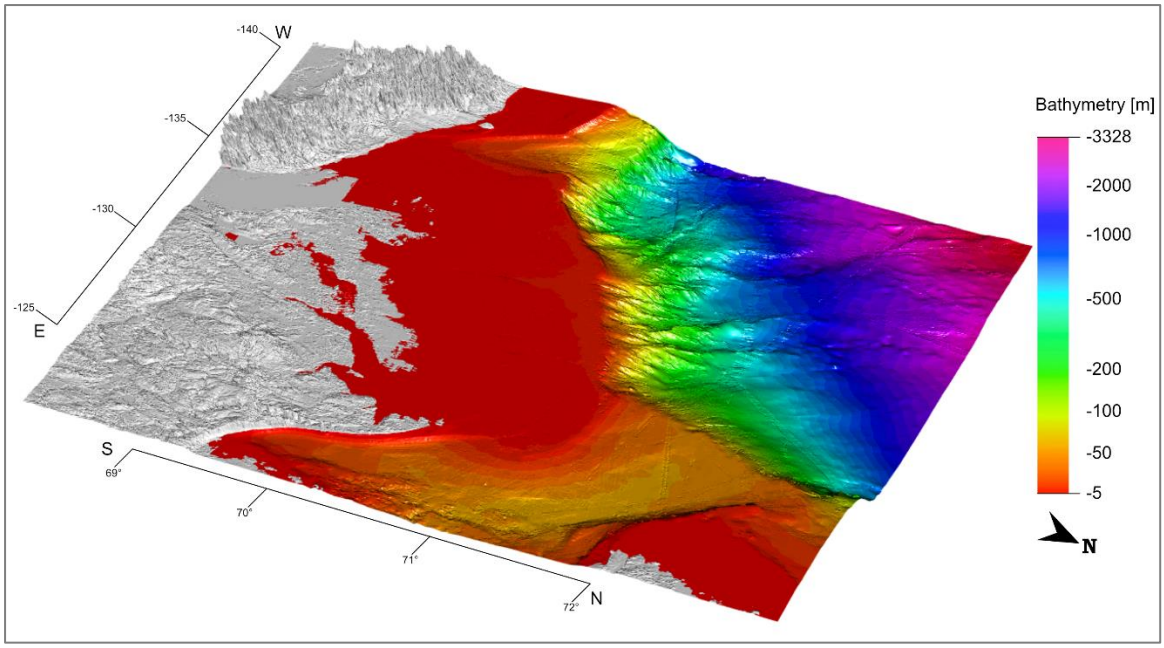

Fig. 2: Bathymetry 3D Modell; based on the GEBCO dataset

The climate is characterized by long, cold winters and short summers: The Sachs Harbor climate station, Northwest Territories on Banks Island, Canada (72°00'00.000" N/ 125°16'00.000" W) measured an average annual temperature of -12.8°C from 1981 to 2010. During the summer (May to September) and winter months (October to April), the average temperature was 0.92°C and -22.5°C, respectively. Annual precipitation in the measured period was 151.5 mm, of which 58.3 mm fell as rain and 97.7 cm as snow (Environment and Climate Change Canada, Government of Canada). Another climate station in Inuvik, Northwest Territories, Canada (68°18'15.000" N/ 133°28'58.000" W) measured an average annual temperature of -8.2°C during the same period. During the summer and winter months, the average temperature here was 8.2°C and -19.9°C, respectively. Annual precipitation during the measured period was 240.6 mm, including 114.5 mm of rainfall and 158.6 cm of snow (Environment and Climate Change Canada, Government of Canada). During the open water season, winds blow mainly from E and NW directions, while NW winds are more common in August and September, as storms are more frequent (Hill and Nadea 1989). Although the Beaufort Sea fetch lengths can be up to 1000 km long and wave heights can exceed 4 m, which furthers coastal erosion, sediment input to the Beaufort Sea from coastal erosion is low compared to the input from the Mackenzie River (Hill et al. 1991).

3. Material and Methods

3.1. PeCaBeau 2021 Expedition and Sample Collection

Sampling was conducted as part of the Permafrost Carbon in the Beaufort Sea (PeCaBeau) Expedition of the Research Vessel CCGS AMUNDSEN (AMD2104) from September 09 to October 07, 2021 (report available here). The aim of the expedition was to record the movement and transformation of material from thawed permafrost along the transition between land and ocean in the southern Beaufort Sea. This includes quantification of the origin of the material, which is derived from coastal erosion of permafrost, Mackenzie River runoff, and submarine permafrost degradation. Sampling was conducted in the southern Beaufort Sea with additional stations in the Amundsen Gulf and McClure Strait (Fig. 3). The ship route focused on five main transects that traversed the shelf from nearshore shallow sites (≤ 20 m) to shelf break and deep waters along the slope, and one transect along the Mackenzie Trough. At the respective locations (marked with red dots in Fig. 3), various samples were collected including deep coring, water column profiling and sediment sampling. Important for this study are the PCB samples, which are listed in the Tab.1 (see Appendix).

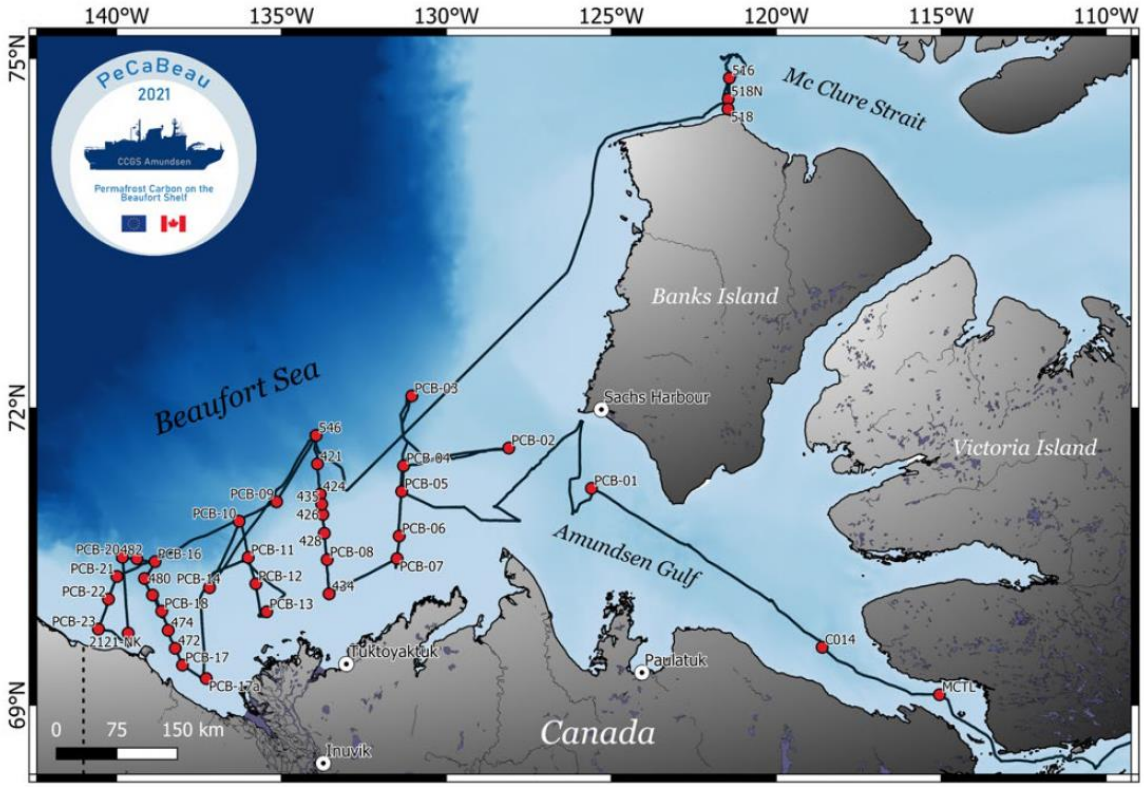

Fig. 3: Map of the study area with cruise track outlined in black and sampling stations marked with red dots (Bröder et al. 2021)

At these locations, among others, a multicorer (MUC) was used to collect multiple sediment samples simultaneously. A major advantage of the MUC is the often undisturbed sediment-water interface it collects during sampling. This is done by the MUC drilling up to eight PVC liners 60 cm long and 10 cm in diameter into the seafloor. The instrument itself weighs between 300 and 400 kg, is 3 m wide and 3.5 m high (Fig. 4). To achieve the desired penetration depth in the seafloor, up to 10 individual lead weights (about 10 kg) can be attached to the core head; in very soft sediments, these lead weights must be removed to avoid overfilling the liner tubes. Once the rack touches down on the seabed, the core head is pushed into the sediment by its own weight (Fig. 5). After sediment removal, spring-loaded closures are pressed onto the tubes from above and below to secure the samples. Back on deck, cores were removed and secured. The respective tubes from each MUC were further used for a diverse purpose. In general, four tubes were cut open at 1-2 cm intervals to perform sediment properties, quantitative element and biomarker analyses. These were cut open by the Benthos lab on the ship, bagged, and frozen at -20°C. The other tubes were either archived or used for pore water analyses and solid phase geochemical sampling.

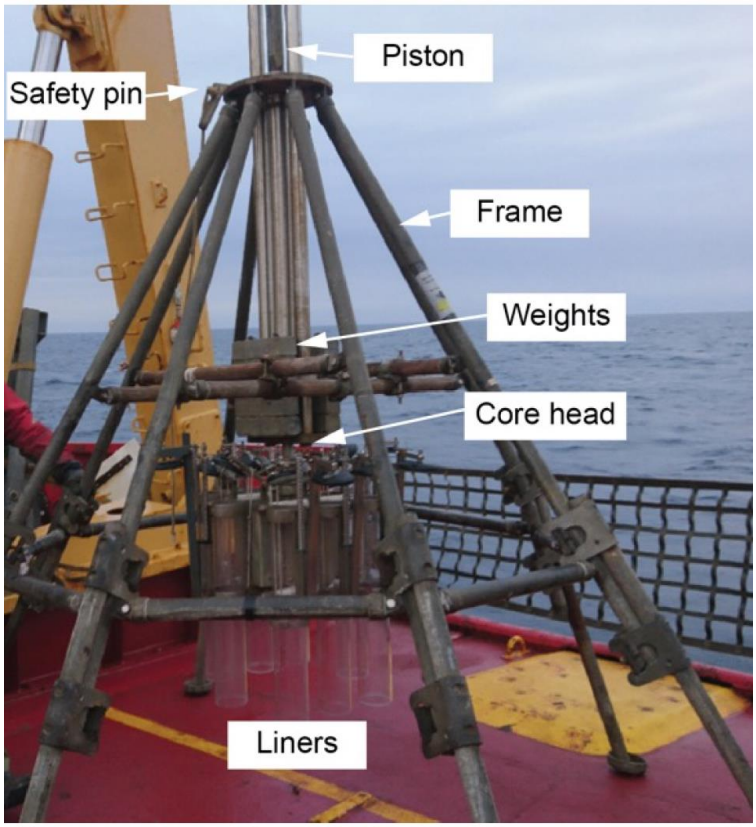

Fig. 4: Multicorer from AWI Bremerhaven on deck the CCGS Amundsen before deployment (Bröder et al. 2021)

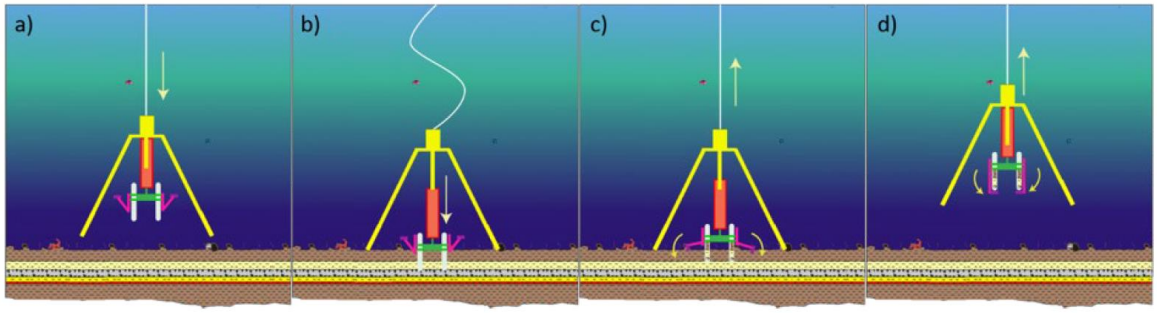

Fig. 5: Schematic of multicorer sampling the seafloor with a) descent, b) contact: liners sink into the sediment, c) retract: tension on wire triggers arms to close tubes, d) recovery (illustration by Daniel Rudbäck, Bröder et al. 2021)

3.2. Laboratory Analysis

3.2.1. Sample Preparation for Sediment Analysis

The samples of the MUC short cores were splitted on board of the Amundsen icebreaker, frozen and then transported to the AWI Potsdam, Germany. At the laboratory they were weighed frozen, then freeze-dried and afterwards weighed again for calculating the water content (Tab. 2, see Appendix). Within the context of this thesis, only the upper two centimeters (0-1 cm and 1-2 cm) were further investigated. For this purpose, the samples were splitted again. One part was used for grain size analysis, the other was milled using a planetary mill. The exact workflow can be seen in Fig. 6. The measured laboratory results are listed in Tab. 3 (see Appendix).

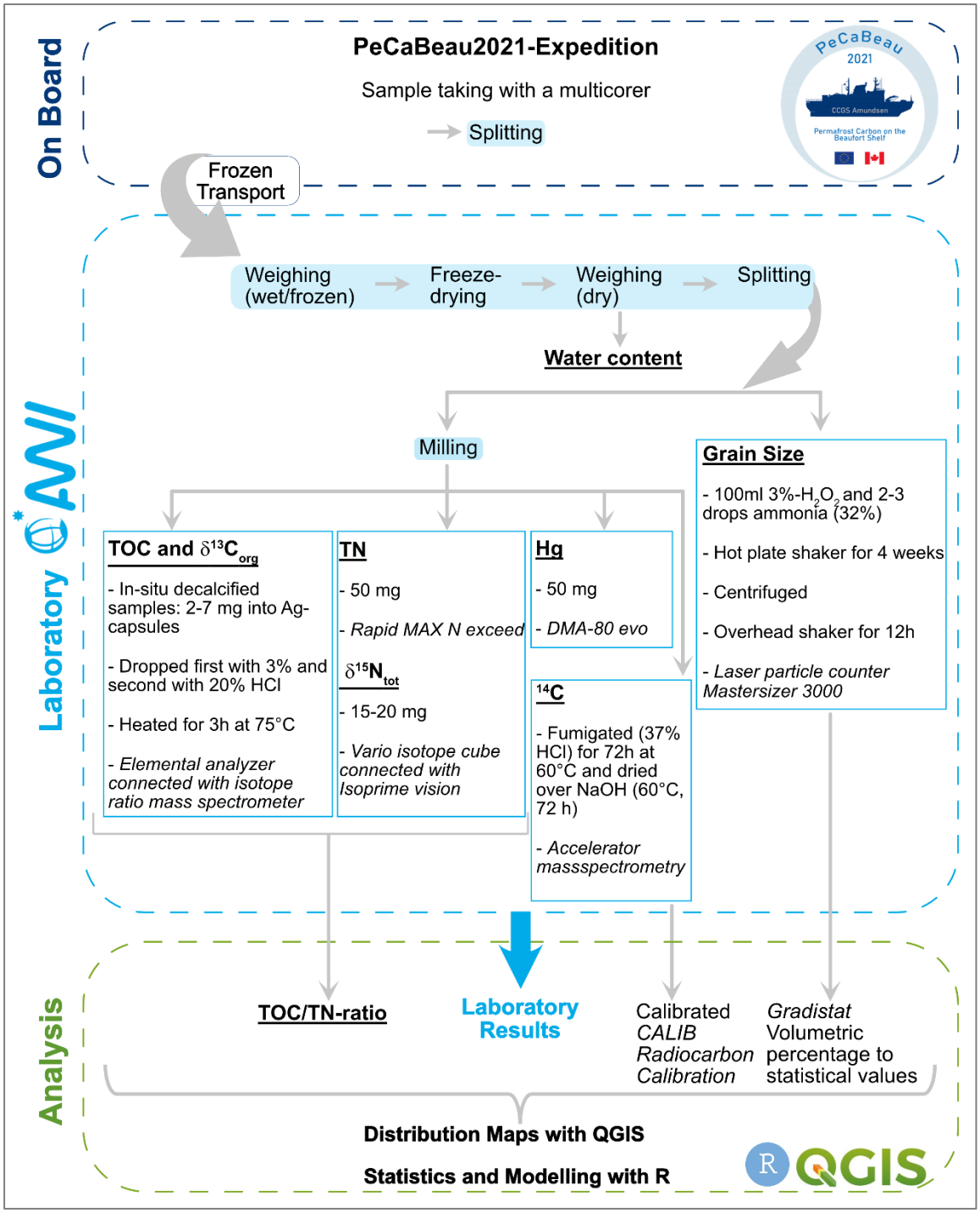

Fig. 6: Workflow and Sample Preparation

3.2.2. Grain Size Determination

For the grain size determination, the samples were made up with 100 ml of 3 %-H_2O_2 and 2-3 drops of ammonia (32 %) for removing all organic remains. Then they were put on a hot plate shaker for four weeks and afterwards centrifuged. Later 0.6 g were weighed in with tetrasodium pyrophosphate for grain dispersal and put on an overhead shaker for 12 h. Measuring of the grain size took place with a Laser particle counter Mastersizer 3000 (*MALVERN*).

3.2.3. Elemental Determination TOC, $\delta^{13}C_{org}$ / TN, $\delta^{15}N_{tot}$ / Mercury

Total Organic Carbon (TOC) and the stable isotope $\delta^{13}C_{org}$ were measured at the GFZ (Geo Forschungs Zentrum) in Potsdam, Germany. The milled samples were in-situ decalcified by weighing in 2-7 mg into Ag-capsules and dropped first with 3 % and second with 20 % HCl. Afterwards they were heated for 3 h at 75°C and measured with an elemental analyzer (*FlaschEA1112*) connected with a ConFloIV interface on a DELTA V IRMS (isotopic ratio mass spectrometer, *ThermoFischer Scientific*).

For the determination of Total Nitrogen (TN) 50 mg of the milled samples were weighed in and measured with rapid MAX N exceed (*ELEMENTAR*). For the measurement of the stable isotope $\delta^{15}N_{tot}$, 15-20 mg milled sample material was weighed into Sn-capsules and measured with a vario isotope cube connected with a Isoprime vision (*Elementar Analysesysteme GmbH*) at the laboratory for soil science and geoecology at the Eberhard Karls university in Tübingen, Germany.

Mercury (Hg) content was determined by weighing in 50 mg of the milled samples and measuring with a DMA-80 evo (*MWS-GmbH*). The results are given in the unit µg kg^{-1}.

3.2.4. ^{14}C-Dating

Age dating of the bulk sediments was completed by the radiocarbon method at the ETH (Eidgenössische Technische Hochschule) in Zurich, Switzerland. Here for the milled samples were acid fumigated (37 % HCl) for 72h at 60°C and dried over NaOH (60°C, 72 h). Afterwards the samples were measured with an accelerator mass spectrometry (Mini Carbon Dating System MICADAS, Ionplus, Dietikon, Switzerland).

3.3. Data Evaluation/ Statistical Analysis

3.3.1. IDW-Interpolation

Spatial surface interpolation techniques in a geographic information system (GIS) are practical tools for calculating unknown surface values (Lam 1983). Inverse distance weighting is a mathematical interpolation method and is used for interpolation of the spatial dependence of georeferenced data. It is a common interpolation method in environmental mapping (Lancianese and Dinelli 2015). The basic assumption is that the similarity of an unknown value to the known measured value decreases with distance from the target, i.e. the further apart the data are, the less similar they are (Bartier and Keller 1996). The unknown points are calculated by multiplying the measured value by a weight that is proportional to the inverse of the distance between the estimation point and the measurement location (Chen and Liu 2012):

$$z(x_0) = \frac{\sum_{i=1}^{n} \frac{z_{xi}}{d^m(x_0 x_i)}}{\sum_{i=1}^{n} \frac{1}{d^m(x_0 x_i)}}$$

To apply the method in QGIS (Version 3.16.2), it is first necessary to determine how many sample points are to be used for the calculation. This can be done using two approaches: a radius distance from a point to be determined and a number of points (ESRI 2022). In the first approach, the user can specify a radius around point x, whereupon the algorithm randomly selects a number of points within the specified radius. In the second approach, the user can specify how many points around the point x should be used for the calculation, so that based on an algorithm, the number of points closest to the point x is calculated (ESRI 2022). The efficiency of this approach depends on how regular the sampling grid is, as interpolation of data with too low density can lead to unrealistic results (Lancianese and Dinelli 2015). For the following distribution maps, the first approach was used. The advantages of this interpolation method are that (1) it allows a very fast calculation for large-area surfaces, (2) different distances are considered in the estimation, and (3) the influence of the distance can be controlled by the distance weighting exponent (Li 2021). However, the method should also be considered critically. For instance, no directional weighting is possible, i.e., spatial relationships are not included (e.g., elevation points along a ridgeline or depositional processes along stream networks) (Spadoni 2006). Furthermore, it is assumed that minimum and maximum values are already known. Therefore, the interpolated values always lie in the value range in between and hence cannot reflect real extreme or outlier values. Moreover, IDW is known to be sensitive to outliers in the dataset, i.e. extreme values can have a significant impact on the interpolated surface,

potentially leading to inaccurate results (Li and Heap 2011). In addition, the inaccuracy of the interpolated areas in the following distribution maps is very high due to the large distances between the sampled sites. Since other parameters such as bathymetry and currents that affect sediment distribution and deposition are not included in the interpolation, the calculated values are further distorted. Therefore, the following created distribution maps serve only as a graphical visualization. The interpolated values are neither considered in the description of the results nor in the discussion. Hence, only the measured values at the sample stations will be discussed in the following.

3.3.2. Spatial Analysis

Using the distance tool in QGIS, the distance of the PCB stations to the coast of northern Canada and the Mackenzie Delta were calculated. The exact water depth at the sample stations was measured during sampling. In addition, based on the GEBCO 2022: North Polar region (Gridded Bathymetry Data Download) dataset, the bathymetry 3D model of the study area was created using R software (Version 4.2.0) with the packages: *rgdal* (Bivand et al. 2023), *rgl* (Murdoch and Adler 2023), and *reshape2* (Wickham 2007).

3.3.3. Grain Size

With the package Gradistat (Blott and Pye 2001) size distribution and further statistical parameters were calculated. From this, the average values of every PCB station between the centimeters 0-1 and 1-2 were calculated, respectively. The median grain size (D_{50}) values were used for the distribution map as well as for the percental deviation and for the correlation matrix.

3.3.4. TOC/TN/Hg/ Stable Isotopes

The calibration for TOC and $\delta^{13}C_{org}$ was performed using an elemental (Urea) and certified isotope standard (USGS24, IAEA-CH-7) and checked with a soil reference sample (Boden3, HEKATECH). The reproducibility for replicate analyses is 0.2 % for TOC and 0.2 ‰ for $\delta^{13}C_{org}$. TN was checked with a reference standard (EDTA 5:45 dilution) and $\delta^{15}N_{tot}$ was calibrated based on a multi-point calibration with international standards (IAEA-600, NSVEC). Hg values were checked with a reference standard (BCR-142R light sandy soil) of the Joint Research Centre of the European Commission. Based on those values, the average values of the two centimeters were calculated respectively for each parameter. Moreover, the C/N ratio (atomic) was calculated with the following formula, with the values of the individual centimeters as well as with the average values, respectively:

$$C/_N\, Ratio = \frac{TOC}{TN} * 1.167$$

3.3.5. ^{14}C-Dating

For the radiocarbon dating of the bulk sediments, the measured data was calibrated using the CALIB Radiocarbon Calibration (Stuiver and Reimer 1993). The median was then selected from the calibrated year range for every PCB station respectively. In addition, the average values of the two centimeters were calculated based on the respective median values. The data is given in years before present (yrs BP).

4. Results

4.1. Sediment Composition and Spatial Distribution

4.1.1. Grain Size

The median grain size in 0-1 cm depth ranges from 2.97 (PCB16) to 71.88 µm (PCB22). The sampled sediment is mainly fine silt, where values range from 2.97 (PCB16) to 6.22 µm (PCB17a). Station PCB23 is the only one in the category with medium silt at 8.74 µm, PCB5 is coarse silt at 50.18 µm, and PCB22 is fine sand at 71.88 µm. In 1-2 cm depth, the median grain size ranges from 3.01 (PCB3) to 19.45 µm (PCB5). Compared to the centimeters on top, some stations have more coarse grain, and others have finer grain. The percentage deviation is shown in Fig. 16. Here, the stations PCB5 and 22 stand out in particular, since they are 61.2 % and 78.1 % finer grained, respectively, in the second centimeter than in the first centimeter. In the depth of 1-2 cm all stations except PCB5, 22, and 23 are fine silt. The remaining three stations have a median grain size that ranges from 8.64 (PCB23) to 19.45 µm (PCB5) and are therefore classified as medium silt.

Fig. 7 shows the volume distributions of the grain size of the average values of the respective PCB stations. Almost all stations have a very similar curve shape, with the peak (>4 %) in the fine silt and the largest volumetric fraction between coarse clay and medium silt. PCB5, 22 and 23 represent exceptions. PCB5 has a 2.2 % volumetric fraction in the fine silt, but the peak is clearly in the medium sand at 5.9 %. PCB22 has no clear peak in the distribution, instead having a mixing of all grain size fractions between medium clay and coarse sand. There is a larger proportion of fine silt with 2.1 % as well as a peak in medium sand with 2.9 %. PCB23 also has no clear peak. The largest volumetric proportion (3 %) lies between the grain sizes medium silt and coarse silt. In contrast to PCB22, the sand fraction is lower here (1.1 % and descending in fine sand). No more material is present above a grain size of 600 µm.

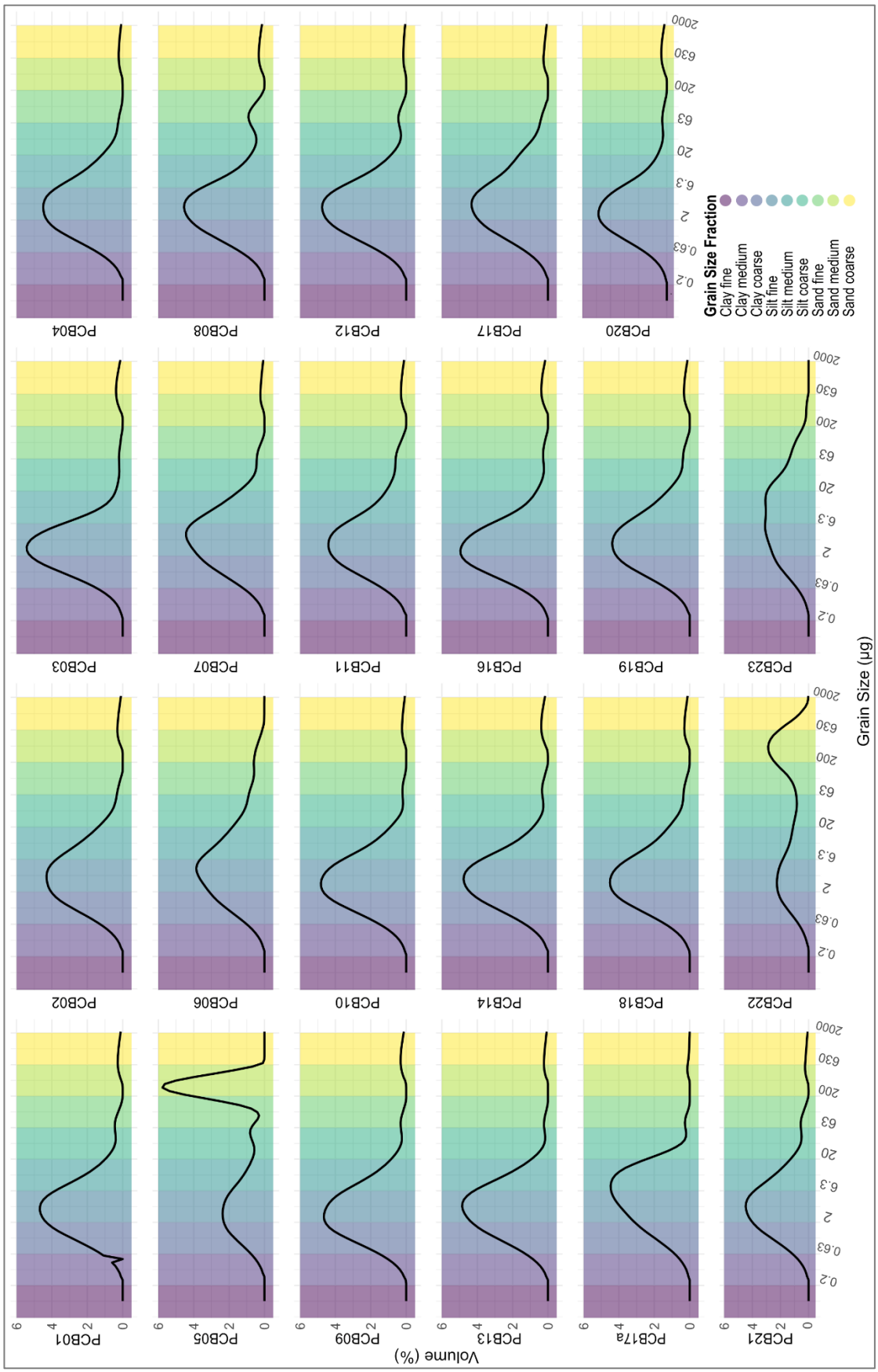

Fig. 7: Volume Distribution of Grain Size

In Fig. 8 the spatial distribution of median grain size interpolated from the 0-1 and 1-2 cm averages is shown. Here it is shown that the fine silt material (2.0-6.3 µm) is distributed in Amundsen Gulf, the deeper Beaufort Sea, the Mackenzie Trough, and on the shelf adjacent to the Kugmatite Valley. The material at the Mackenzie delta is medium silt grained (6.3-20.0 µm) as are stations PCB6 and 7, which are still on the shelf. Stations PCB5 and 22 are both located directly at the shelf break and stand out as the only stations in the coarse silt grain size (34.81 and 43.83 µm, respectively).

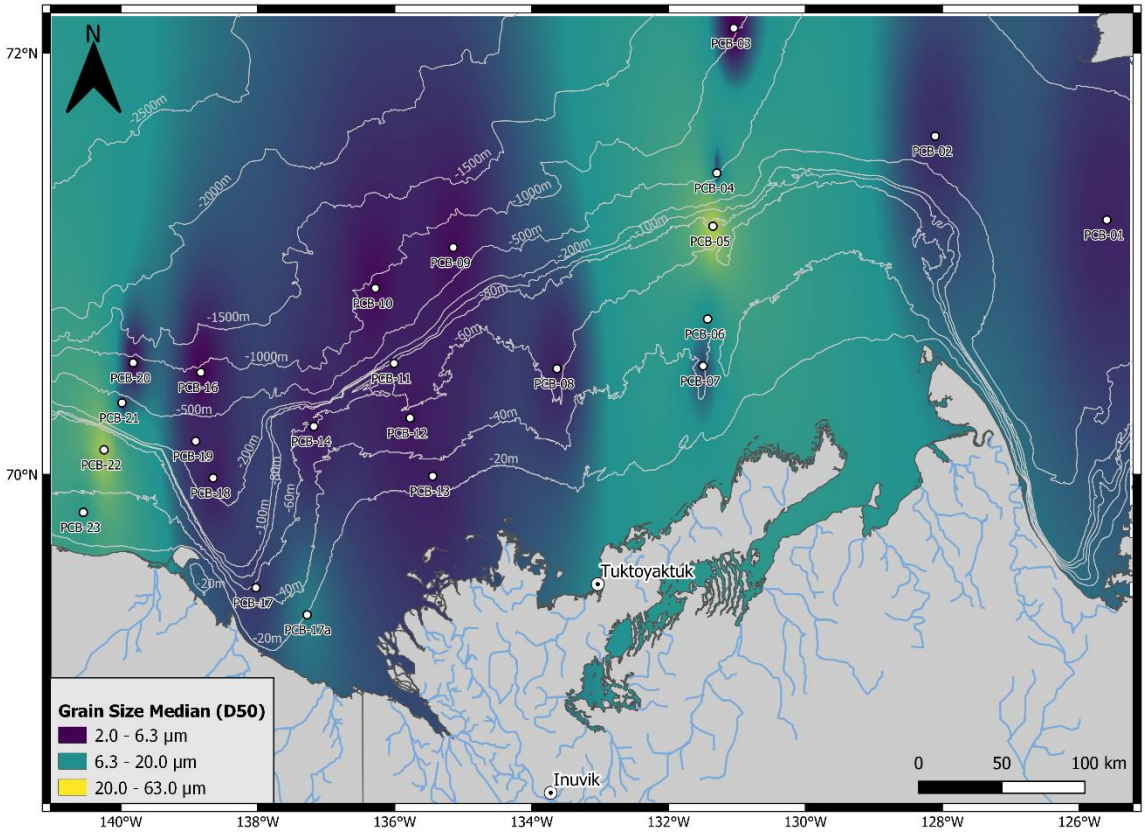

Fig. 8: Interpolated Distribution Map of Grain Size (D50)

4.1.2. Total Organic Carbon

TOC values range from 0.6 (PCB22) to 1.7 % (PCB8) at 0-1 cm depth and from 0.6 (PCB22) to 1.6 % (PCB7/12) at 1-2 cm depth. This limits the TOC content in the surface sediments to less than 2 %. Based on Fig. 16, which shows the percent deviation between the centimeters, the values within the two centimeters do not differ much from each other, except at station PCB23, where the TOC content at 0-1 cm depth is 1.3 % and at 1-2 cm depth is 1.1 %, resulting in a percent deviation of -15.8 %. The remaining deviations are between +5 and -10 %. Spatially, TOC distributes unevenly (Fig. 9). Most TOC (1.5-1.7 %) is found between 40 and 60 m depth, in the Kugmatite Valley, as well as between the Mackanzie Delta and Herschel Island. Less TOC (1.3-1.4 %) is found on the rest of the shelf as well as north of the shelf break, in the Mackenzie Trough and in Amundsen Gulf. Carbon content between 1.1 and 1.2 % is found at stations PCB23, which is very close to shore, as well as PCB3, which is located in the Beaufort Basin. 1 % and less TOC is measured at stations PCB5 and 22.

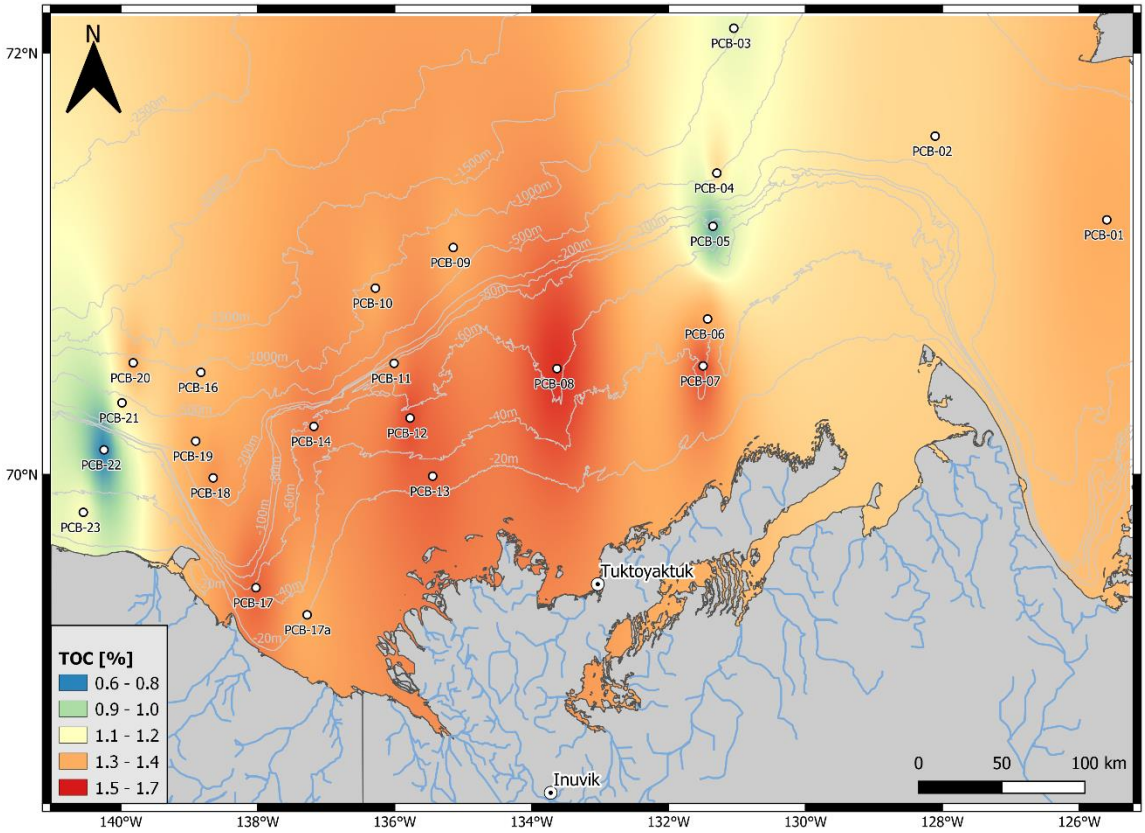

Fig. 9: Interpolated Distribution Map of Total Organic Carbon

4.1.3. Total Nitrogen

Measured TN ranges from 0.13 to 0.28 % at 0-1 cm and from 0.10 to 0.26 % at 1-2 cm depth, respectively at stations PCB22 and PCB8. The percent variation between the two depths is shown in Fig. 16. Here the values vary from 19.7 (PCB7) to -28.4 % (PCB23). The spatial distribution of the average values of the two centimeters (Fig. 10) is comparable to the carbon distribution. Most of the measured TN (0.23 - 0.26 %) is found in the Kugmallit Valley (PCB8) and at the stations PCB7 and 12, which are located in 60 m water depth. In the surrounding area on the shelf, as well as at stations PCB9 and 10, which are located northern the shelf break, the values range between 0.19 and 0.22 %. In the Amundsen Gulf and the Mackenzie Trough less TN is measured (0.16-0.18 %). The lowest measured TN (0.11-0.15 %) is found in the sediments at stations PCB5 and 22, which are located directly at the shelf break as well as at PCB17a, directly at the Mackenzie Delta.

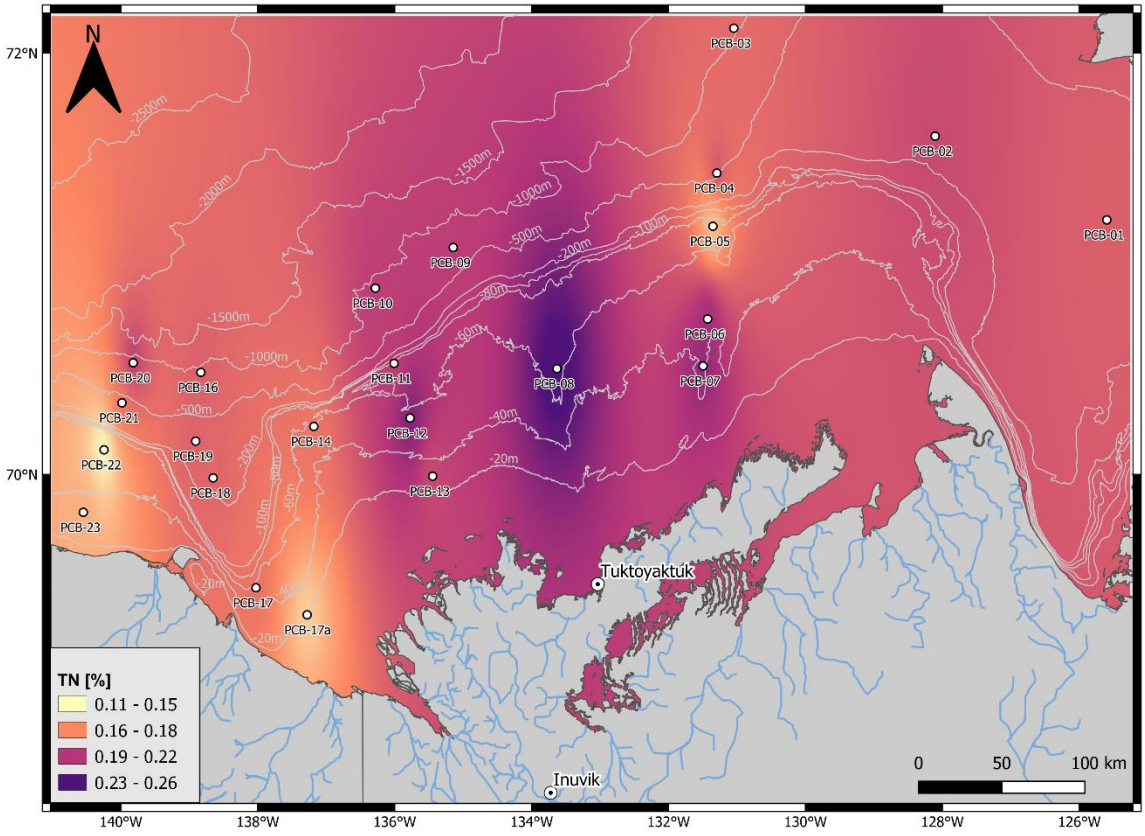

Fig. 10: Interpolated Distribution Map of Total Nitrogen

4.1.4. C/N ratio

The C/N ratio averaged 7.99 with a minimum of 5.41 (PCB22) and a maximum of 11.71 (PCB17a) at 0-1 cm depth and with an average of 8.09 from 6.76 (PCB5) to 11.35 (17a) at 1-2 cm depth. The percent variation between centimeters can be seen in Fig. 16. Station PCB22 stands out, with a 38.7% higher C/N ratio at 1-2 cm depth than at 0-1 cm. On the map of the spatial distribution of the average values of the two centimeters (Fig. 11), higher ratios (>10) accumulate at the Mackenzie Delta. In addition, stations PCB7 and PCB23 also have higher (>8.6) C/N ratios. In the rest of the study area, C/N ratios range from 7.1 to 8.5, except for stations PCB5 and 22, which both have ratios <7.

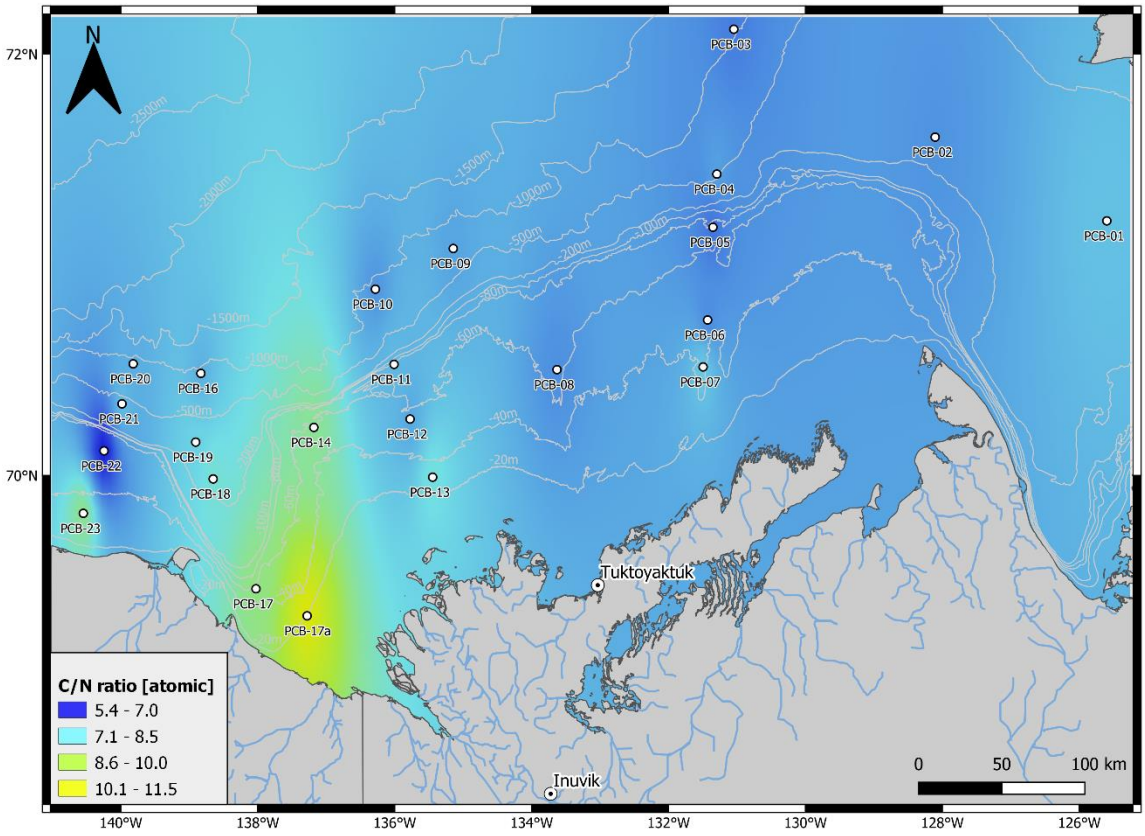

Fig. 11: Interpolated Distribution Map of C/N ratios

4.1.5. Mercury

Measured Hg values range from 36.06 (PCB22) to 110.84 µg kg^{-1} (PCB10) in 0-1 cm depth and from 45.03 (PCB22) to 110.53 µg kg^{-1} (PCB16) in the centimeter beneath. The percentage deviation between the first and second centimeter can be seen in Fig. 16. Almost all of the values in the two depths do not differ strongly from each other. The stations PCB4 (7.7 %), PCB19 (-8.2 %) and PCB22 (24.9 %) are the only ones that are outstanding, with >5 % deviation. In the spatial distribution (Fig. 12), which was created using the average values, a spatial pattern can be observed: Hg increases with the water depth. The lowest values are found at the stations PCB5 (52.51 µg kg^{-1}) and 22 (40.55 µg kg^{-1}) as well as at station PCB23 (63.49 µg kg^{-1}). On the remaining shelf, the average values range from 79.78 (PCB7) to 96.81 µg kg^{-1} (PCB12). Behind the shelf break, the measured Hg amount is between 102.34 (PCB4) and 110.13 µg kg^{-1} (PCB11).

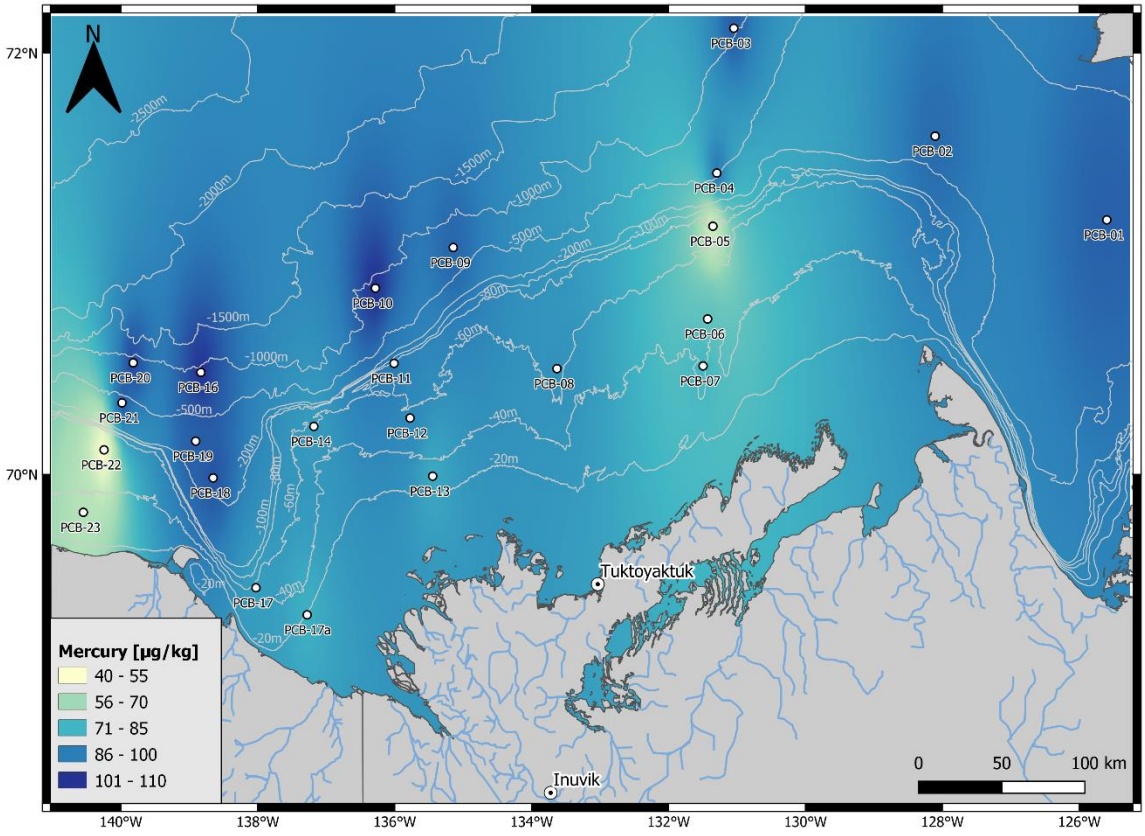

Fig. 12: Interpolated Distribution Map of Mercury

4.1.6. $\Delta^{13}C_{org}$

The stable carbon isotope ($\delta^{13}C_{org}$) ranges from -26.4 (PCB17a) to -23.8 ‰ (PCB3) in the upper centimeter and from -26.4 (PCB17a) to -23.6 ‰ (PCB3) in the lower centimeter. The percent deviation is shown in Fig. 16. Here, the values differ by less than one percent, resulting in the two centimeters being almost identical. The average values and their spatial distribution are visualized in the following map (Fig. 13). A clear accumulation of low $\delta^{13}C_{org}$ values (-26.4 to -25.5 ‰) can be seen at the Mackenzie Delta. On the rest of the shelf, as well as north of the shelf break, the values range from -25.4 to -24.3 ‰. The highest values measured (-24.2 to -23.6 ‰) are located in the Amundsen Gulf.

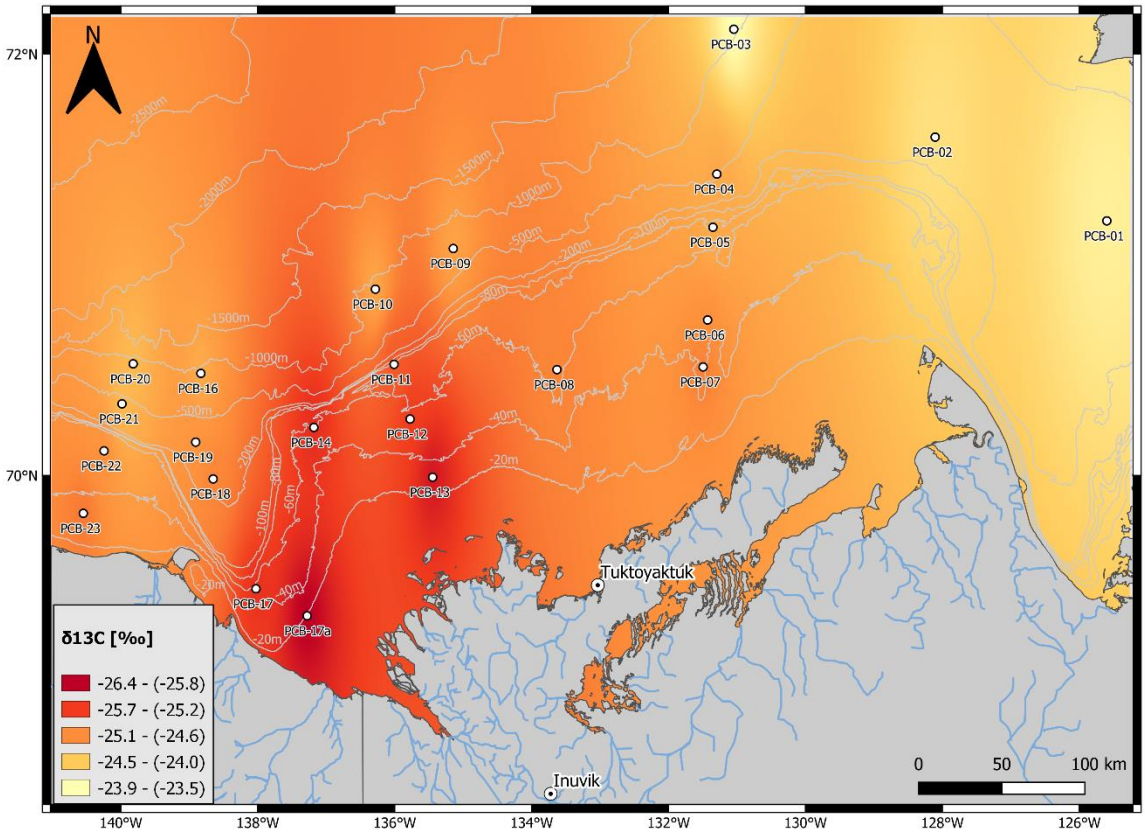

Fig. 13: Interpolated Distribution Map of $\delta^{13}C_{org}$

4.1.7. $\Delta^{15}N_{tot}$

The values of the stable nitrogen isotope ($\delta^{15}N_{tot}$) were calibrated and range between 3.82 (PCB17a) and 7.86 ‰ (PCB22) in 0-1 cm depth. In 1-2 cm depth the lowest value is 3.70 (PCB17a) and the highest 7.67 ‰ (PCB1). The percent deviation between the two centimeters (Fig. 16) is between -11.9 % at PCB23 and 9.2 % at PCB21. The spatial distribution of the average value (Fig. 14) shows that the lowest measured values (between 3.7 and 5.6 ‰) accumulate at the Mackenzie Delta. Stations PCB7 and 23, which are located on the shelf, have values <6.6 ‰. Throughout the rest of the study area, the values are at >6.6 ‰. The highest $\delta^{15}N_{tot}$ values are located in the Amundsen Gulf (>7.0 ‰) and at PCB22 (7.48 ‰).

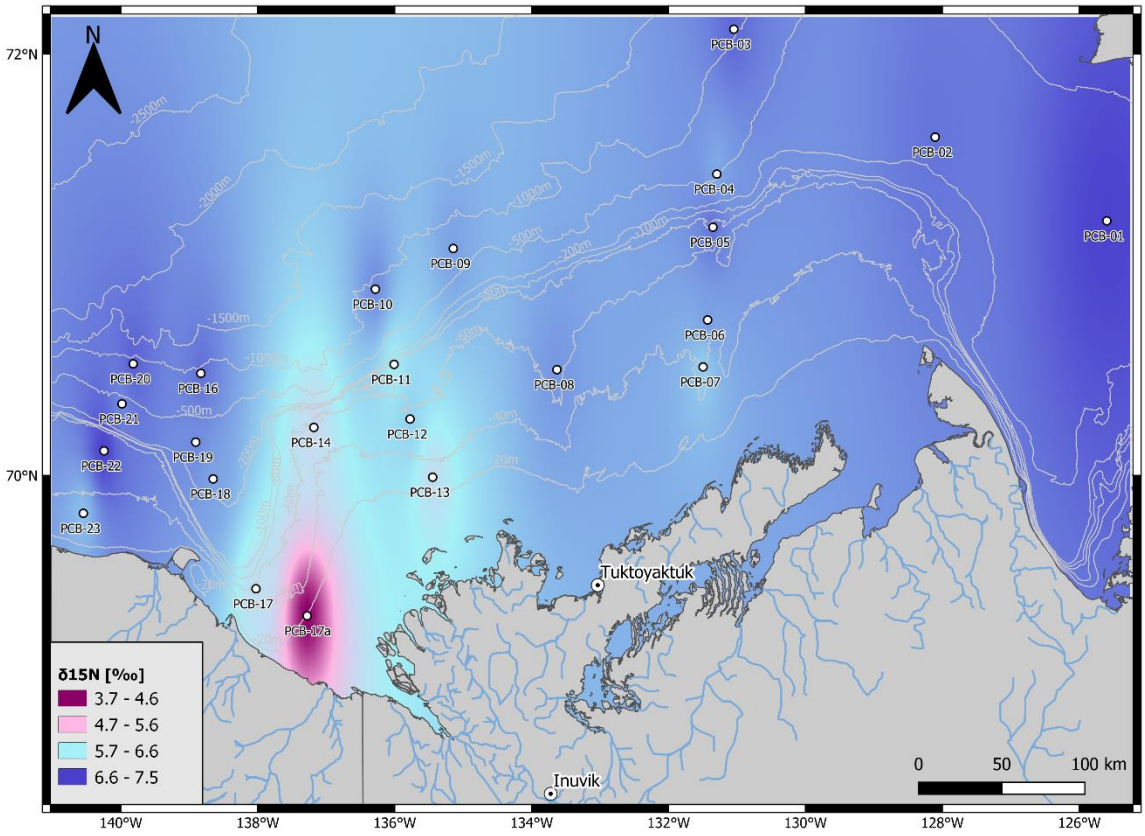

Fig. 14: Interpolated Distribution Map of $\delta^{15}N_{tot}$

4.1.8. Bulk sediment age

At 0-1 cm depth the bulk age ranges from 5560 (PCB1) to 10223 yrs BP (PCB17a). At 1-2 cm depth, values range from 4294 (PCB5) to 10794 yrs BP (PCB14). The difference (in years) between the two depths can be seen in Fig. 16. Here it is shown that the stations PCB2, 4, 5, 7, 8, 17a, 22 and 23 have material, which is younger in 1-2 cm than in the centimeter above. Station PCB5 is particularly outstanding, as its material is 2171 years younger in 1-2 cm than in 0-1 cm. The spatial distribution of the two-centimeter averages (Fig. 15) shows that the oldest measured material (between 8500 and 10000 yrs BP) accumulates around the Mackenzie Delta (PCB17a, 17, 14, 13). North of the shelf break (PCB4, 9, 10), material is deposited that is between 7500 and 8000 years old. In the Mackenzie Trough and western of Herschel Island, as well as in the deeper Beaufort Sea (PCB3), material is younger (between 6500 and 7500 yrs BP). In the Kugmallit Valley as well as at the eastern shelf and in the Amundsen Gulf, the youngest sediments were sampled.

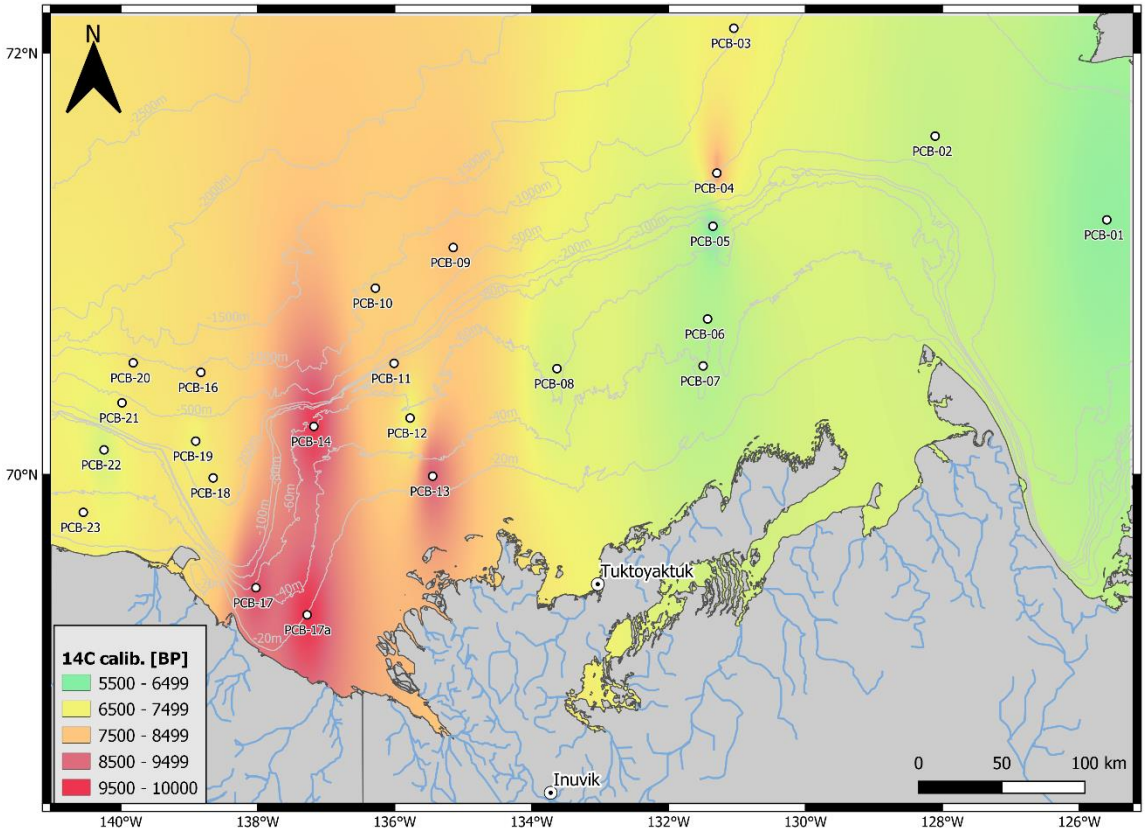

Fig. 15: Interpolated Distribution Map of $\delta^{14}C$

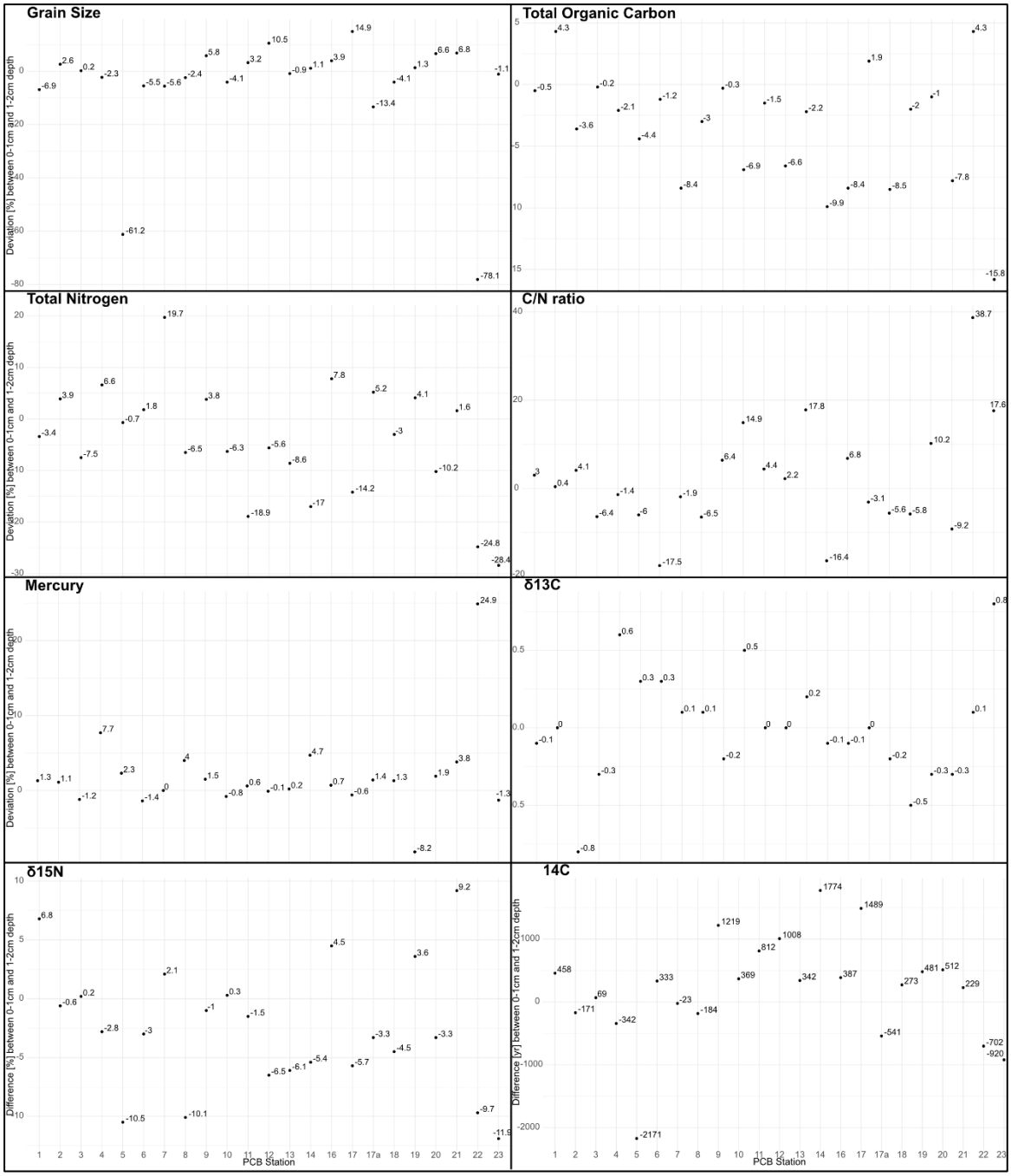

Fig. 16: Percentage Deviation between samples in 0-1 and 1-2 cm depth

4.2. Correlation Matrix

In order to better understand the relation between the individual parameters, a correlation matrix is used (Fig. 17). Fig 17 (a) shows the correlation of the average values of the two depths (0-1 and 1-2 cm). Relations including distance to coast and water depth or distance to Mackenzie Delta are autocorrelated, and therefore also show strong positive correlation coefficients (0.71 and 0.69, respectively). Therefore, they are not discussed further below. Those parameters are only included in the matrix to examine their influence on the individual study parameters in more detail. Another autocorrelation is given for TN and TOC (0.80), meaning with increasing carbon more nitrogen is present in the material. Particularly strong negative correlations are found for grain size with Hg content (-0.85) as well as for grain size with TOC (-0.84) and TN (-0.69), respectively.

Other strong correlations are present between Hg and TOC (0.65), TN (0.64), and water depth (0.6). In addition, the ^{14}C data correlate with C/N ratios (0.60), $\delta^{13}C_{org}$ values (-0.61), and $\delta^{15}N_{tot}$ (-0.71). $\delta^{13}C_{org}$ values also correlate with distance to coast (0.70), water depth (0.67), distance to delta (0.79), C/N ratio (-0.61), and very strongly with $\delta^{15}N_{tot}$ (0.86). Moreover, $\delta^{15}N_{tot}$ has a high negative correlation coefficient with C/N ratios (-0.82).

Fig. 17 (c) and (e) show the correlations in the actual centimeters. With some exceptions, they do not differ much. The only stronger differences involve the parameters ^{14}C, C/N ratio and $\delta^{15}N_{tot}$. In particular, the correlation coefficients between grain size and ^{14}C (-0.19 and -0.55), C/N ratio (-0.49 and -0.12), and $\delta^{15}N_{tot}$ (0.43 and 0.08) change in 0-1 and 1-2 cm, respectively. In addition, the correlation coefficient between Hg and ^{14}C (0.08 and 0.41), C/N ratio (0.25 and -0.10) and $\delta^{15}N_{tot}$ (-0.15 and 0.17) changes within the two depths. Further noticeable change is present in the correlation between TOC and ^{14}C (0.15 and 0.42).

Fig. 17 (b), (d), and (f) each show the same correlation matrices as already described, but the two stations PCB5 and 22 were removed from the data set since they are particularly outstanding with salient values in many parameters.

When stations PCB5 and 22 are removed from the correlation matrix (Fig. 17 (b)), new stronger correlations become visible compared to the matrix with the whole data set, while on the other hand some parameters are no longer strongly correlated. For example, there is a strong correlation between the C/N ratio and the TN content (-0.73), which, however, did not exist when the whole data set is considered. Other newly appearing correlations are TOC and water depth (-0.55), grain size and distance to coast (-0.58), and Hg with $\delta^{15}N_{tot}$ (0.5). In contrast, correlations decrease for the following parameters: Grain size and

TN from -0.69 (total data set) to -0.45 (outlier removed) or for grain size and TOC from -0.84 to -0.24. Similarly, for the parameters Hg with TN and TOC. Here the values change from 0.64 to 0.22 and 0.65 to -0.11, respectively. A particularly strong change is present with the correlation coefficient between grain size and C/N ratio. In the complete data set the correlation coefficient is -0.42, in the modified data set 0.48. Apparently, stations PCB5 and 22 have a very strong influence: For example, considering the complete data set, it can be assumed that with finer grain size there is a higher C/N ratio. This assumption is refuted as soon as stations PCB5 and 22 are not taken into consideration. Here it can be supposed that the C/N ratio also increases with increasing grain size. Overall, the described changes can also be seen in the respective centimeters (Fig. 17 (c,d,e,f)).

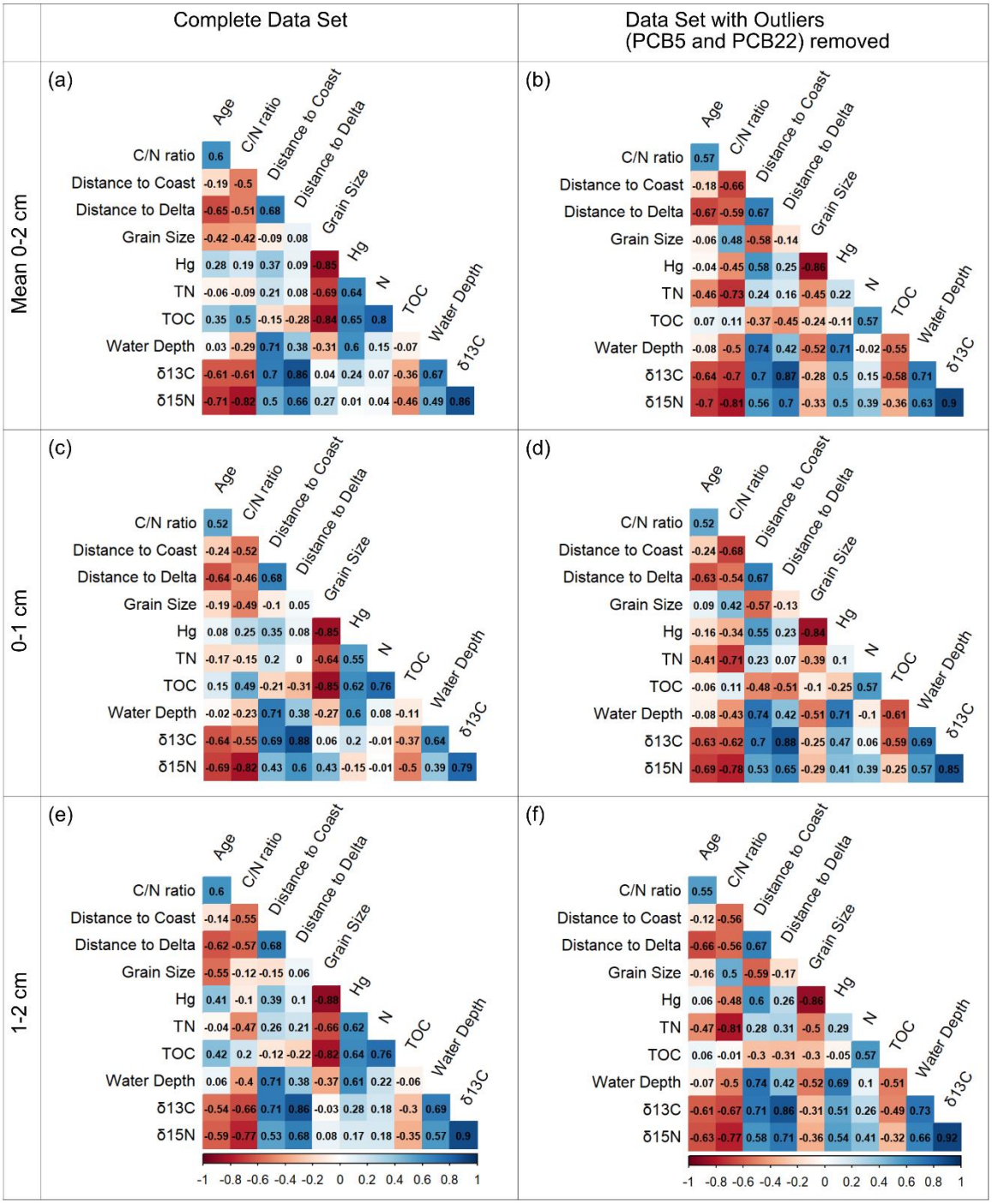

Fig. 17: Correlation Matrix

4.3. Dual-Carbon Isotope Endmember Modelling

Fig. 18 shows isotopic modeling of $\delta^{13}C_{org}$ with $\delta^{15}N_{tot}$ (Fig. 18 (a)), C/N ratio (Fig. 18 (b)), and 14C (Fig. 18 (c)) with spatial grouping where each PCB station is located in the study area. An individual clustering of the spatial categorization is visible. In each plot, there is a clustering of stations in the Amundsen Gulf that have the highest measured $\delta^{13}C_{org}$ values (-23.7 to -24.1‰) and $\delta^{15}N_{tot}$ values (6.91-7.43 ‰) as well as are in the lower measured value range in both C/N ratio (7.00-8.04) and bulk age dating (5789-7656 yrs BP). The Behind Shelf Break stations also cluster with $\delta^{13}C_{org}$ values between -24.5 and -24.8 ‰ along to higher $\delta^{15}N_{tot}$ values (6.34-7.11 ‰), lower C/N ratios (7.37-7.98), and comparatively older bulk ages (7868-8981 yrs BP). Another grouping, although not as dense in concentration, are the PCB stations on the Mackenzie Delta and in its immediate area of influence. Here, $\delta^{13}C_{org}$ values range from -25.4 to -26.4 ‰ with the lowest measured $\delta^{15}N_{tot}$ values (3.76-5.96), a very wide range of C/N ratios (7.64-11.53), and the oldest bulk material (7338-9953 yrs BP). A clear outlier in all three plots is PCB17a, located directly at the delta with either the highest measured values in $\delta^{13}C_{org}$, C/N ratio and ^{14}C or the lowest in $\delta^{15}N_{tot}$. The remaining stations, which are grouped into Beaufort Shelf, Mackenzie Trough and Yukon Coast, also cluster, although not as clearly as the groups already described. Here all stations are in the middle range of the measured $\delta^{13}C_{org}$ values (-24.7 to -25.2 ‰) as well as in the other measured parameters. Station PCB5 stands out as it has both a higher $\delta^{13}C_{org}$ and $\delta^{15}N_{tot}$ value compared to the other stations in the Beaufort Shelf group as well as the youngest bulk material.

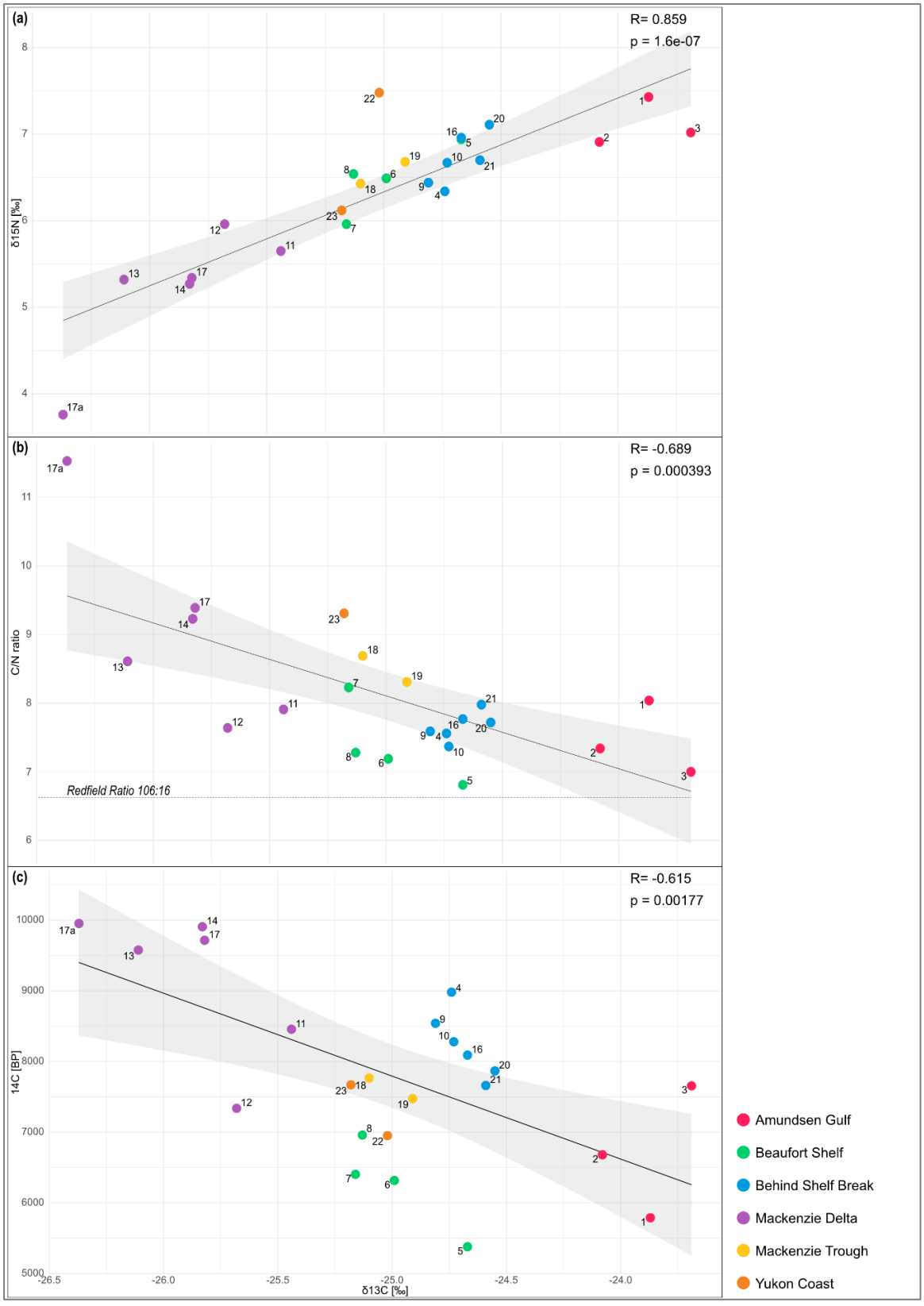

Fig. 18: Dual-Carbon Isotope Endmember Modelling

5. Discussion

5.1. Origin of Organic Matter

Terrestrial OM mainly originates from freshwater plankton and vascular plants, to which erosive and depositional processes contribute soil OM of various ages (Coffin et al. 2017). Marine OM is predominantly of autotrophic and heterotrophic origin (Magen et al. 2010). The deposition, accumulation, and burial of OM in sediments is an important component of the carbon cycle in nearshore shelf systems (Vonk et al. 2014). The relative contribution of terrestrial and/or marine OM to sedimentary carbon pools can be defined by determining C/N ratio and stable isotope ($\delta^{13}C_{org}$ and $\delta^{15}N_{tot}$) composition (Lamb et al. 2006). Based on these data, estimates of the relative contribution of each source can be made.

Previous studies in the Arctic have found that OM derived from terrestrial sources has $\delta^{13}C_{org}$ values in the range of -28 to -25 ‰ (Naidu et al. 2000; Semiletov et al. 2011; Vonk et al. 2012) and $\delta^{15}N_{tot}$ range from 0 to 5.0 ‰ (O'Brien et al. 2006). Given the reference values of the stable isotopes, the results can be divided into groups based on predominant OM sources (Fig. 19). Group A includes material with low $\delta^{13}C_{org}$ (<-25 ‰) and low $\delta^{15}N_{tot}$ (<6 ‰) due to high amounts of heterotrophic production fed by allochthonous OM, terrigenous carbon, and/or freshwater phytoplankton (O'Brien et al. 2006). The main sources of this organic carbon (OC) are freshwater POC and DOC, and C_3 land plants (Vonk et al. 2012). Group A consists only of sediments located at the mouth of the Mackenzie River and the direct area of influence of the Mackenzie plume, where the Coriolis force directs the plume towards the east of the river delta (Bell et al. 2016). According to Goñi et al. (2000), river sediments have a $\delta^{13}C_{org}$ signature of -26.2 to -26.9 ‰. Using this range of values, it can be determined that OC at stations PCB17a (West Channel) and PCB13 (East Channel) originates from the Mackenzie River. With increasing distance to the delta, $\delta^{13}C_{org}$ values also increase (r value = 0.86, Fig. 17 (a)). Therefore it can be assumed that terrestrial OM (OM_{terr}), derived from the Mackenzie surface plume, is detached from the freshwater plume by subsidence and gets carried away by the water masses of the Beaufort Sea (Osborne and Forest 2016). Sedimentary OC is enriched with autochthonous marine OC as a function of water depth (Kim et al. 2022). This mixing between freshwater of the Mackenzie and ocean waters, and the subsequent deposition of the material, results in $\delta^{13}C_{org}$ and $\delta^{15}N_{tot}$ values matching the isotopic ranges of terrestrial and marine organic end members. Those PCB stations are grouped together as group B, which includes the samples that are influenced by both, terrigenous carbon, and marine production. OM_{terr} can be transported to the shelf break and beyond into the Beaufort basin as a long-term

storage (Forest et al. 2007; Letscher et al. 2013). Further offshore, the input of autochthonous sources increases along the shelf and towards the Beaufort Sea, where autochthonous production prevails (Naidu et al. 2000). Group C includes sample stations that are located offshore at higher salinities and have high $\delta^{13}C_{org}$ (> -24) and $\delta^{15}N_{tot}$ (> 6.9) values, indicating high cell growth rates of marine phytoplankton and/or ice algae, and relatively low dilution by terrigenous matter (O'Brien et al. 2006; Coffin et al. 2017).

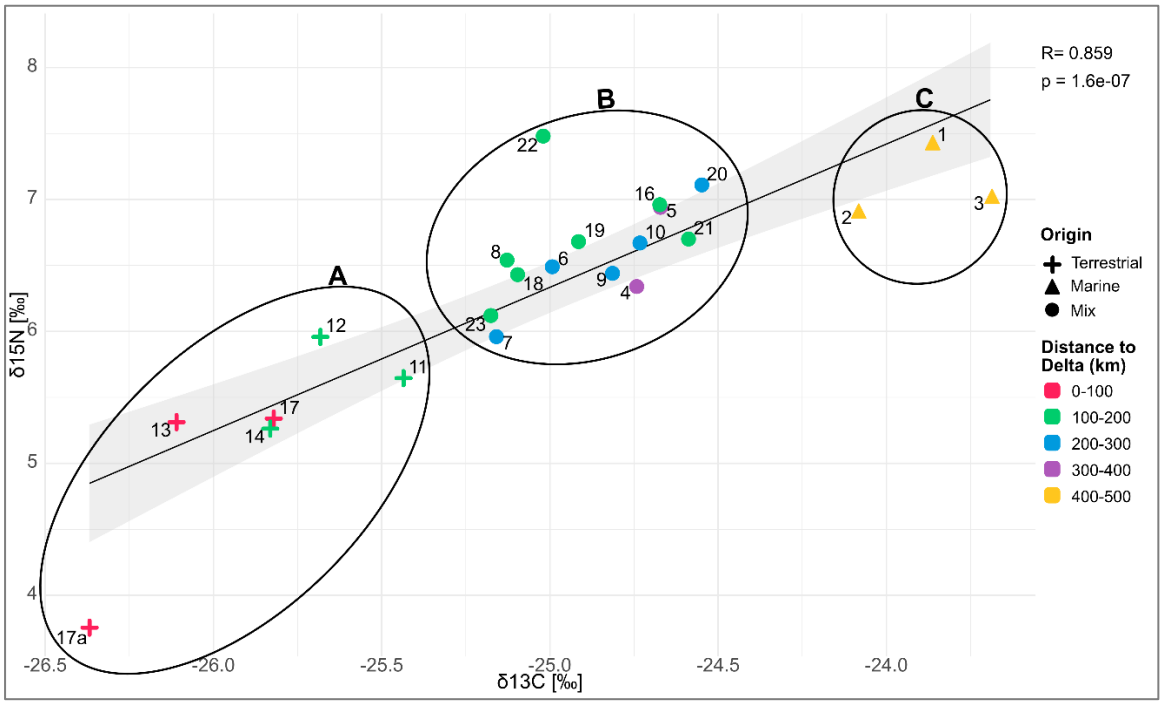

Fig. 19: Stable Isotope Endmember Modelling

Moreover, the measured C/N ratios are generally very low (Fig. 11). The ratio of terrestrial plants is usually >15, whereas the C/N ratio of phytoplankton ranges between 4 and 10 (Bell et al. 2016). Therefore, the low ratios of <10 across the study area (except PCB17a) do not indicate strong influence of and mixing with OM_{terr}. However, those findings are inconsistent with the low $\delta^{13}C_{org}$ and $\delta^{15}N_{tot}$ values already discussed, which show a clear signature of terrestrial material on the shelf. Moreover, the measured C/N ratios are above the Redfield Ratio (Fig. 18 (b)), indicating the presence of an essential terrestrial organic component (Ruttenberg and Goñi 1997). One reason for the low C/N ratios could be the low percentage of buried TOC (≤1.7 %). Rivers transport 4.4 Mt yr^{-1} TOC into the Beaufort Sea (Rachold et al. 2004), while the contribution from coastal erosion is between 4.9 to 14 Mt yr^{-1} (Wegner et al. 2015). However, OM is rapidly degraded during the coastal erosion process, in relation to greenhouse gas emissions (Tanski et al. 2017). Especially CO_2 release depends on the availability of fresh and degradable organic material (Tanski et al. 2021). In this process, sediments eroded in thaw slump systems may remain onshore for

years to decades before being released into the ocean (Cray and Pollard 2015). This transit time can result in large OC loss (up to 50 %), with release of CO_2 before being transported into the Beaufort Sea (Tanski et al. 2019). Moreover, Couture et al. (2018) found that only 0.004 Mt (12.2 %) of organic carbon eroded from coastal sediments of the Yukon coast is bound in nearshore sediments.

Another reason for the low C/N ratios could be the effect of nitrogen associated with mineral phases, causing the marine contribution to be overrepresented (Schubert and Calvert 2001). In clay-rich sediments with high amounts of illite (clay mineral primarily responsible for binding of ammonium), it is important to distinguish between organic and bound inorganic nitrogen (Winkelmann and Knies 2005). Ammonium, which is formed during the remineralization of organic material, is easily adsorbed onto clay mineral surfaces, and is subsequently protected from microbial use (Müller 1977; Stevenson 1994). Based on Schubert and Calvert (2001), almost 50 % of the total nitrogen in the surface sediments of the central Arctic Ocean consist of this inorganic fraction. Therefore, they suggest using TOC/N_{org} values for the interpretation of OM sources in the Arctic. However, since only the TN content was measured in the laboratory and no extraction was made, there are no values regarding the inorganic or organic nitrogen content. Surface sediments in Spitsbergen are also affected by inorganic nitrogen, resulting in low TOC/TN ratios (5-15) compared to TOC/N_{org} (8-49) (Winkelmann and Knies 2005). Due to the high clay content (between 12.9 and 33.9 %) in the sediments examined in our study and the high correlation between TN and grain size (r value = -0.69), we can assume that the unusual low C/N ratios are caused by the content of inorganic nitrogen.

Another possibility that offers more information about the origin of OM is the bulk radiocarbon age. ^{14}C signature of marine OM is a marker for modern, pre-aged, or fossil carbon and thus provides information about the source of OM, especially when combined with additional stable isotopes measurements (Faust et al. 2023). ^{14}C contents correlate with both $\delta^{13}C_{org}$ (r value = -0.61) and $\delta^{15}N_{tot}$ (r value = -0.71). Fig. 15 shows a clear accumulation of old bulk material around the Mackenzie River delta and on the inner shelf, representing a clear OM_{terr} input, associated with erosion of Holocene sediments from the Mackenzie River. Bulk age decreases with increasing distance to the shore from about 10223 to 5560 yrs BP, supporting the assumption of increasing proportions of autochthonous marine OM with younger ^{14}C ages in sedimentary OM (Kim et al. 2022). CO_2 used by phytoplankton for marine primary production is only marginally depleted in ^{14}C compared to atmospheric CO_2 (Linick 1980). Therefore, marine surface sediments containing predominantly marine OM (OM_{mar}) are not highly depleted in ^{14}C (Kim et al. 2011).

In summary, the data from isotopic analysis, as well as radiocarbon dating, indicate that the OM pool of Beaufort Sea sediments consists of a mixture of three end members: OM_{terr}, OM_{mar}, and mixed. In this context, the Mackenzie River provides most of organic sediments, as evident from the decrease in the proportion of OC in the surface sediments with increasing distance from the coast. This is supported by the low $\delta^{13}C_{org}$ values and higher C/N ratios at the delta, indicating a large depositional flux of OC, derived from C_3 terrestrial plants. However, because of the unusually low C/N ratios, probably due to the increased proportion of inorganic nitrogen, a determination of origin could not be made using this parameter. Considering the end-member analysis being based on only two parameters, the proportion in the mixed group and therefore the uncertainties are large. In addition, the radiocarbon content of bulk sediments at the mouth of the river indicates a significant terrigenous contribution derived from either petrogenic and/or prehistoric terrestrial deposition, matching the characteristics of the Mackenzie River drainage basin. However, since there are almost no reference values for distinguishing between material derived from the Mackenzie River or from permafrost coastal erosion, it is not possible to make an accurate distinction of those terrestrial endmembers, except for the two stations located directly at the mouth of the Mackenzie River. Further uncertainties within the endmember modeling, especially in the mixed group, can be minimized if additional biomarker analyses are included.

5.2. Spatial Relationships and Distribution

Thawing of coastal permafrost, coastal erosion, and river runoff release sediments in the nearshore zone that are influenced by seasonal dynamic processes (ice cover and river flow), bathymetry, wind, and ocean currents. The released material can be (1) mineralized and emitted as greenhouse gases, (2) deposited as nearshore sediments, and/or (3) transported further offshore by waves, currents, and ice (Fritz et al. 2017; Couture et al. 2018; Tanski et al. 2019). In addition to the different sources of the material, different transport mechanisms can lead to distinct spatial distribution. Those processes include entrainment and transport by sea ice (Eicken et al. 2005), transport in the water column with resuspension (Lalande et al. 2009), and transport through eddies (O'Brien et al. 2013) and currents (Hill et al. 1991; Dmitrenko et al. 2016).

The results and spatial distribution maps suggest a three-way partition in the distribution of material: Mackenzie River runoff with sediments directed to the east of the delta by Coriolis force and westerly winds (Forest et al. 2007), the area behind the shelf break, and the area western of Herschel Island. This is particularly evident in the distribution of TOC (Fig. 9), TN (Fig. 10) and Hg (Fig. 12). On the one hand, this is related to the origin and

whether the material originates from coastal erosion or from the Mackenzie Delta, but on the other hand bathymetry and the associated currents influence the distribution strongly.

Hg content increases with increasing water depth (r value = 0.71, outliers removed, Fig. 17 (b)) and accumulates especially behind the shelf break (> 100 µg kg^{-1}). However, stations PCB5 and 22, which are directly located at the shelf break, stand out in particular, with very low levels of Hg (≤ 55 µg kg^{-1}). These two stations also stand out in the spatial distribution of TOC and TN, with the lowest measured values. Moreover, these are the only stations with a coarser grain size in comparison to the other measured stations (Fig. 8). It can be concluded that OM is bound to fine-grained material (r value = -0.69 for TN and -0.84 for TOC), as fine-grained material has larger surface area and therefore higher OM loading capacity than coarser material (Hedges and Keil 1995). Moreover, Hg is also very strongly negatively correlated with grain size (r value = -0.85), due to the larger surface area, resulting in better binding capacity of heavy metals (Chakraborty et al. 2015). An explanation for these outlier stations could be currents eroding fine-grained material near the shelf edge (Fig. 20). Forest et al. (2016) found that current surges developing at about 10-15 km width on the upper slope of the Mackenzie Shelf, lead to erosion events of surface sediments. Thereby, a velocity of 18 cm s^{-1} represents a threshold value to resuspend silty sediments at the shelf edge, explaining the remaining sandy material. If the critical shear stress for all the different grain sizes is not exceeded, selective transport occurs, i.e., sorting sediments out (Radosavljevic et al. 2022). A further reason for the transport of surface sediments at the shelf edge, is the water flowing down the shelf in winter, in addition to the wind-driven transport during downward events (Forest et al. 2007). Overall, high hydrodynamic energy appears to be present at these two locations, resulting in transportation of finer and rich in OM sediments.

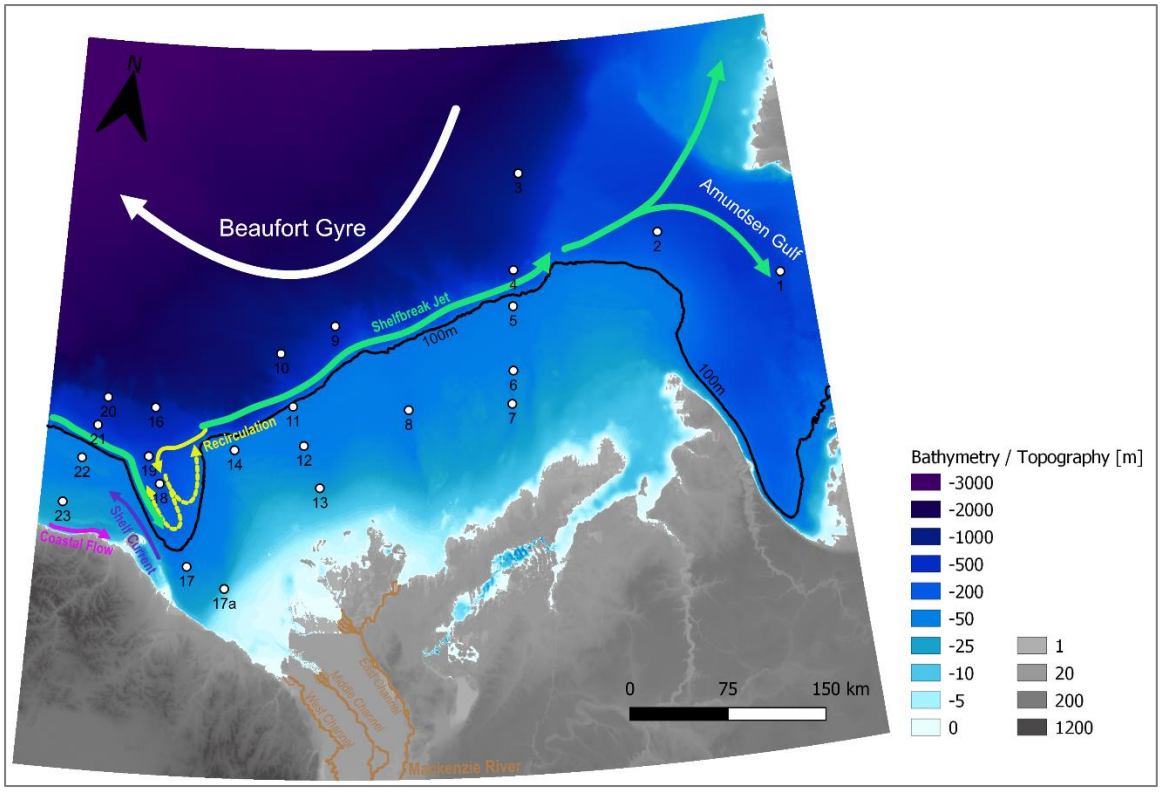

Fig. 20: Map of the Canadian Beaufort Shelf with Influencing Currents, based on Dunton et al. 2006; Dmitrenko et al. 2016; Forest et al. 2016

Another influence of bathymetry on the distribution of OM is evident at stations PCB6, 7, 8, and 12: those are located in troughs on the shelf and, compared to the other stations, are particularly enriched in TOC and TN (> 1.5 and > 0.26 %, respectively). Sedimentation rates are generally much higher on continental shelves than in the central basins, especially in areas of high river input (Wegner et al. 2015). The rates for the Mackenzie shelf sediments range from 0.1-3.0 mm a^{-1}, with the highest rates in the Kugmallit and Ikite troughs (Harper and Penland 1982). This indicates that the troughs function as sediment traps, with accumulation of fine and organic-rich material. A considerable amount of terrigenous material was also found in sediment traps at the shelf edge in other studies (O'Brien et al. 2006). Due to this increased accumulation, microbial degradation is minimized, resulting in more efficient burial (Goñi et al. 2013). This fast deposition is also reflected in the comparatively young bulk age (5500-6500 yrs BP). These sediment traps are also of additional importance when OM is efficiently deposited in the seafloor and buried in the sediments, removing carbon from the carbon cycle (Grotheer et al. 2020).

At the mouth of the river, the material is medium silty and therefore more coarse-grained than on the rest of the shelf or in Amundsen Gulf. The sediment supply on the shelf is largely influenced by the Mackenzie River (Deschamps et al. 2018), indicating an input of less clay-material. Subsequently, waves and storm-generated currents, with velocities of

2-25 cm s^{-1}, result in near-bottom sediment transport from the shore surface to nearshore depths (Lintern et al. 2013). Depending on the flow regime, sediments from the same source, but with different grain sizes, are deposited at different locations along the land-to-ocean path. Grain size decreases from shore sediments to shelf sediments (Vonk et al. 2015), also indicated with a slight negative correlation between grain size and distance to coast (r value = -0.58, outliers removed). Overall, sediments near the coast appear to be more affected by impacts such as wave erosion, resuspension, and/or ice sourcing, which eventually limits OM accumulation (Macdonald et al. 1998; Vonk et al. 2012). 55 % of the OC sediment incoming from the Mackenzie are buried on the shelf, implying a loss of 45 % OC in the delta (Vonk et al. 2015). The already discussed low C/N ratios near the shore indicate degradation and a redistribution of permafrost OM. This is supported by the relation between TOC content and grain size and hence light resuspension.

The input and distribution of terrestrial sediments as well as OM fate changed during the Holocene in association with sea level rise, ice melt, inputs from rivers and coastal erosion, sea ice transport, and redistribution of currents (Hill et al. 1991; Hanna et al. 2014). During the early to mid-Holocene, the sediment regime on the Beaufort Shelf shifted from predominant input from rivers to marine deposition due to postglacial sea level rise and marine transgression (Wegner et al. 2015). In addition, significant changes in freshwater flux and surface and bottom water conditions occurred (Andrews and Dunhill 2004). These changes are also reflected in the calibrated ^{14}C bulk ages (Fig. 15), which show that there is an accumulation of sediments from the young Holocene at the river delta and younger bulk age in the surrounding area. In the delta region, the total stored sediment mass, with an average Holocene accumulation rate of about 136-163 Tg/year (Lewis 1988), was three times greater than deposition on the wider shelf (Hill et al. 1991). The Mackenzie drains into a glacially excavated trough, which may have strongly influenced the timing and transport of fluvial material, following the retreat of the Laurentide Ice Sheet (Wegner et al. 2015). After the Holocene sea ice level maximum, modern depositional processes such as seasonality in sea ice formation and river input, enhanced resuspension of surface sediments, and current transport developed (Macdonald 2000).

To summarize, input and distribution of sediments changed through the Holocene and are influenced by bathymetry and currents. Troughs function as sediment traps of organic rich material with low decomposition. Moreover, currents near the shelf break erode fine grained material, which is rich in OM and higher amounts of Hg, remaining coarser grained sediments with low amounts of TOC, TN and Hg.

5.3. Mobilization and Sedimentation of Mercury

Since the late 1970s, permafrost temperatures have increased globally by 0.5 to 2°C (Biskaborn et al. 2019). With a projected loss of permafrost between 6 to 29 % for every additional 1°C of warming (Koven et al. 2013), elements and compounds are released in addition to climate-relevant greenhouse gases. These include nutrients (Beermann et al. 2015) but also contaminants such as Hg (Dastoor et al. 2022). Hg is a naturally occurring element and is mobilized by volcanism or weathering of continental rocks (Streets et al. 2011). It is bound to the surface layer of permafrost soils for millennia (Mu et al. 2019) and thereby, strongly bound to OM (Schuster et al. 2018). Especially Arctic rivers export large amounts of OC and Hg to the Arctic oceans (Mu et al. 2019). In the Mackenzie River, particulate and dissolved Hg concentrations correlate positively with DOC age, implying that processes releasing older carbon are also an important source of Hg (Leitch et al. 2007). Another important source of Hg into the Beaufort Sea is coastal erosion (Outridge et al. 2008; Soerensen et al. 2016), where the flux will likely increase as erosion rates increase during the 21st century (Irrgang et al. 2018). In total, it is assumed that about 76 Mg Hg year $^{-1}$ are transported to the Arctic shelf areas by rivers or coastal erosion (Soerensen et al. 2016; Sonke et al. 2018). Further important sources of Hg into the Arctic Ocean are from anthropogenic origin from lower latitudes by the atmosphere (Obrist 2007).

For the distribution and concentration of Hg in surface sediments along the Beaufort Shelf and in the basin, grain size is a crucial factor. The finer the grain size of the material, the more Hg is bound (r value = -0.85). The same observation was found in other studies in the Arctic (Fox et al. 2014; Tatsii and Baranov 2022; Kohler et al. 2022). Thereby, the larger specific surface area of clay-silt particles increases the binding of heavy metals to these particles (Chakraborty et al. 2015). The stations with the lowest measured Hg values are PCB5 and 22 (> 55 µg kg^{-1}). These are also the only stations with sandy grain size. As discussed earlier, due to their location on the shelf edge, these stations are exposed to currents that carry away very fine and organic rich material (Fig. 20), leaving sandy material which is less able to bind Hg.

Another crucial factor in the distribution of Hg is the content of TOC (r value = 0.65) and TN (r value = 0.64). OM in the finer fractions of the sediment increases the binding ability and concentration of Hg (Fitzgerald et al. 2007). Chakraborty et al. (2015) further found that marine OM likely has a higher affinity for Hg than OM of terrestrial origin. This supports the assumption that Hg increases with increasing water depth, especially after the shelf break (r value = 0.71, outliers removed), whereas the influence of marine OM increases. The uptake of Hg by POM and the deposition of Hg from the euphotic zone derived from

atmospheric deposition probably represent the main source of Hg in deep-sea sediments (Sanei et al. 2021). A further reason for the higher Hg concentrations with increasing water depth could be redistribution of Hg occurring after decomposition of Hg-containing POM, releasing dissolved Hg into the pore water (Fitzgerald et al. 2007). The resulting diffusion and adsorption to iron and manganese hydroxides in surface sediments may lead to Hg enrichment (Fitzgerald et al. 2007; Kohler et al. 2022). Furthermore, it is striking that surface sediments on the shelf have lower concentrations (<100 µg kg^{-1}), despite the close proximity of Hg inputs from coastal erosion and the Mackenzie River, than sediments behind the shelf break. This suggest that wave actions and ice scour are eroding Holocene sediments and transporting material from the shallow regions into the Canada basin (Hare et al. 2008). It can be concluded that the basin is taking up Hg, not exporting it, and therefore acting as a Hg sink. In this context, the accumulation and burial of Hg in surface sediments represents the largest Hg removal mechanism in the Arctic ocean (Dastoor et al. 2022). In eastern Canada, Hg concentrations in surface sediments have been found to decrease since closure due to natural recovery of sediments by recent deposition (Walker 2016). However, weather Hg can become more bioavailable under anoxic conditions, remains open and requires further research.

In summary, a spatial pattern of distribution of Hg in surface sediments was observed. Here, the concentrations are comparable to those found in other areas of the Arctic Ocean. A negative correlation was found between Hg and grain size as well as positive correlations between Hg, TOC and TN. This suggests that the distribution of Hg is determined by the transport of fine-grained sediments and by the uptake of OM and Fe/Mn oxides. Moreover, Hg increases with water depth and accumulates in the Canada basin, suggesting a sink in the Hg-cycle.

5.4. Degradation of Organic Matter

Degradation of OM is influenced by several factors, including matrix protection, chemical lability in relation to its molecular structure, and enzymatic limitations (Karlsson et al. 2015). Isotopic analysis results of $\delta^{13}C_{org}$ and $\delta^{15}N_{tot}$ indicate that most of the Mackenzie-derived material is deposited in the delta and on the shelf (Fig. 19), as well as material originating permafrost coasts, where rapid flocculation and sedimentation likely enhance the preservation of terrestrial OM (Drenzek et al. 2007). The extent of terrestrial OC degradation is dependent on oxygen exposure, which is a function of sediment transport time (Keil et al. 2004) as degradation occurs during transport of terrestrial OC, while the burial efficiency decreases with distance offshore (Kim et al. 2022). This is also shown by the

decreasing C/N ratios with increasing distance from the delta in relation to $\delta^{13}C_{org}$ values (Fig. 18 (b)). Nearshore OM may be degrading rapidly as a result of mineralization by microorganisms (Tanski et al. 2017), as indicated by a decrease in C/N ratio from 11.53 at station PCB17a (located directly at the Mackenzie River delta) to 9.39 at PCB17 (about 30 km northwest). With increasing distance from the delta, the proportion of marine OM increases, which is considered as more labile and therefore more easily degradable than terrestrial OM (Burdige 2007).

As already discussed and shown by other studies in the Beaufort Sea, sediment traps such as basins and troughs on the shelf are very important for long-term carbon storage (Hilton et al. 2015; Couture et al. 2018; Grotheer et al. 2020). Due to the increased accumulation in those traps, microbial degradation is minimized (Goñi et al. 2013). In addition, Hilton et al (2015) found that river-bound POC is more efficiently buried, while OC derived from coastal erosion is preferentially mineralized and thus has a potentially stronger impact on GHG emissions. It can be concluded that permafrost OC is easily degradable (Vonk et al. 2013) as it has been kept frozen and undegraded for millennia (Grotheer et al. 2020).

6. Conclusion

The results of this study show regional differences in the distribution of TOC, TN, as well as their stable isotopes, bulk age, Hg, and grain size in surface sediments of the Canadian Beaufort Sea. These differences reflect variable distribution mechanisms and different sedimentary OM preservation systems. The spatial distributions were cartographically represented using the IDW interpolation method. However, since the study area is very large, the interpolated area is affected by uncertainties; therefore, the maps are used as a graphical visualization, while only the measured values at the PCB stations were interpreted. Based on isotopic analysis of $\delta^{13}C_{org}$ and $\delta^{15}N_{tot}$ sources throughout the study area, three groups can be distinguished: (1) allochthonous material (from rivers and coastal erosion) represents the majority of the Mackenzie shelf sediments, (2) autochthonous material includes organic carbon from marine primary production that can be clearly assigned to the Amundsen Gulf region, and (3) a mixture of both. Due to the unusual low C/N ratios, which are likely caused by the increased proportion of inorganic nitrogen, this parameter could not be used for origin determination. Given the endmember analysis based on only two parameters, the proportion in the mixed group is large. These uncertainties could be mitigated, and more accurate endmembers established if, for example, biomarker analysis was included. Moreover, it was not possible to define precisely which material originates clearly from coastal erosion and which from the Mackenzie River, based on only the stable isotopes of TOC an TN.

Furthermore, bathymetry and currents were found to strongly influence both the distribution and accumulation of OM, Hg, and sediments with different grain sizes. Currents erode fine-grained material that is rich in OM. In addition, troughs on the shelf were found to act as sediment traps where OM accumulates strongly. Moreover, Hg content, which is strongly bound to OM, increases with water depth and accumulates in the Canada basin, which functions as a Hg-sink. Overall, the input and distribution of sediments changed due to changing environmental conditions during the Holocene. Last, OM degradation of terrestrial material was found to occur during transport and thus burial efficiency decreased with increasing distance from shore.

Given these strong regional differences, no unified conclusion can be made about how climate-related changes such as permafrost degradation, increases in fluvial runoff, and decreases in sea ice cover will affect benthic species and biotopes. The influx of OM, both allochthonous and autochthonous, is expected to increase due to higher bio-productivity, increased coastal erosion, and greater sediment resuspension. This will involve increased inputs of terrestrial material, particularly on the shelf. Climate change may also affect the

duration and intensity of freeze-thaw cycles of the tundra, altering the flux of terrestrial OM to the coastal shelf. Finally, changes in sea ice extent and concentration as well as ocean currents may affect sediment transport, which will lead to redistribution of OM in surface sediments.

7. References

Andrews, John T.; Dunhill, Gita (2004): Early to mid-Holocene Atlantic water influx and deglacial meltwater events, Beaufort Sea Slope, Arctic Ocean. In Quat. res. 61 (1), pp. 14–21. DOI: 10.1016/j.yqres.2003.08.003.

Aré, F. E. (1988): Thermal abrasion of sea coasts (part I). In Polar Geography and Geology 12 (1), p. 1. DOI: 10.1080/10889378809377343.

Atkinson, David E. (2005): Observed storminess patterns and trends in the circum-Arctic coastal regime. In Geo-Mar Lett 25 (2-3), pp. 98–109. DOI: 10.1007/s00367-004-0191-0.

Bartier, Patrick M.; Keller, C.Peter (1996): Multivariate interpolation to incorporate thematic surface data using inverse distance weighting (IDW). In Computers & Geosciences 22 (7), pp. 795–799. DOI: 10.1016/0098-3004(96)00021-0.

Beermann, Fabian; Teltewskoi, Annette; Fiencke, Claudia; Pfeiffer, Eva-Maria; Kutzbach, Lars (2015): Stoichiometric analysis of nutrient availability (N, P, K) within soils of polygo-nal tundra. In Biogeochemistry 122 (2-3), pp. 211–227. DOI: 10.1007/s10533-014-0037-4.

Belicka, Laura L.; Harvey, H. Rodger (2009): The sequestration of terrestrial organic carbon in Arctic Ocean sediments: A comparison of methods and implications for regional carbon budgets. In Geochimica et Cosmochimica Acta 73 (20), pp. 6231–6248. DOI: 10.1016/j.gca.2009.07.020.

Bell, L. A.; Bluhm, B. A.; Iken, K. (2016): Influence of terrestrial organic matter in marine food webs of the Beaufort Sea shelf and slope. In Mar. Ecol. Prog. Ser. 550, pp. 1–24. DOI: 10.3354/meps11725.

Biskaborn, Boris K.; Smith, Sharon L.; Noetzli, Jeannette; Matthes, Heidrun; Vieira, Gonçalo; Streletskiy, Dmitry A. et al. (2019): Permafrost is warming at a global scale. In Nature communications 10 (1), p. 264. DOI: 10.1038/s41467-018-08240-4.

Bivand R, Keitt T, Rowlingson B (2023). *rgdal: Bindings for the 'Geospatial' Data Abstraction Library*. http://rgdal.r-forge.r-project.org, https://gdal.org, https://proj.org, https://r-forge.r-project.org/projects/rgdal/.

Blott, Simon J.; Pye, Kenneth (2001): GRADISTAT: a grain size distribution and statistics package for the analysis of unconsolidated sediments. In Earth Surf. Process. Landforms 26 (11), pp. 1237–1248. DOI: 10.1002/esp.261.

Braune, Birgit; Chételat, John; Amyot, Marc; Brown, Tanya; Clayden, Meredith; Evans, Marlene et al. (2015): Mercury in the marine environment of the Canadian Arctic: review of recent findings. In The Science of the total environment 509-510, pp. 67–90. DOI: 10.1016/j.scitotenv.2014.05.133.

Bring, A.; Fedorova, I.; Dibike, Y.; Hinzman, L.; Mård, J.; Mernild, S. H. et al. (2016): Arctic terrestrial hydrology: A synthesis of processes, regional effects, and research challenges. In J. Geophys. Res. Biogeosci. 121 (3), pp. 621–649. DOI: 10.1002/2015JG003131.

Bröder, Lisa; O'Regan, Matt; Fritz, Michael; Juhls, Bennet; Priest, Taylor; Lattaud, Julie et al.: The Permafrost Carbon in the Beaufort Sea (PeCaBeau) Expedition of the Research Vessel CCGS AMUNDSEN (AMD2104) in 2021. In Berichte zur Polar- und Meeresforschung = Reports on Polar and Marine Research 759. DOI: 10.48433/BzPM_0759_2022.

Bröder, Lisa; Tesi, Tommaso; Andersson, August; Eglinton, Timothy I.; Semiletov, Igor P.; Dudarev, Oleg V. et al. (2016): Historical records of organic matter supply and degradation status in the East Siberian Sea. In Organic Geochemistry 91, pp. 16–30. DOI: 10.1016/j.orggeochem.2015.10.008.

Burdige, David J. (2007): Preservation of Organic Matter in Marine Sediments: Controls, Mechanisms, and an Imbalance in Sediment Organic Carbon Budgets? In ChemInform 38 (20). DOI: 10.1002/chin.200720266.

Burn, C. R.; Kokelj, S. V. (2009): The environment and permafrost of the Mackenzie Delta area. In Permafrost Periglac. Process. 20 (2), pp. 83–105. DOI: 10.1002/ppp.655.

CALIB rev. 8; Stuiver, M., and Reimer, P.J., 1993, Radiocarbon, 35, 215-230.

Carmack, Eddy C.; Macdonald, Robie W. (2002): Oceanography of the Canadian Shelf of the Beaufort Sea: A Setting for Marine Life. In ARCTIC 55 (5). DOI: 10.14430/arctic733.

Castello, Leandro; Zhulidov, Alexander V.; Gurtovaya, Tatiana Yu; Robarts, Richard D.; Holmes, Robert M.; Zhulidov, Daniel A. et al. (2014): Low and declining mercury in arctic Russian rivers. In Environmental science & technology 48 (1), pp. 747–752. DOI: 10.1021/es403363v.

Chakraborty, Parthasarathi; Sarkar, Arindam; Vudamala, Krushna; Naik, Richita; Nath, B. Nagender (2015): Organic matter — A key factor in controlling mercury distribution in es-tuarine sediment. In Marine Chemistry 173, pp. 302–309. DOI: 10.1016/j.marchem.2014.10.005.

Chen, Feng-Wen; Liu, Chen-Wuing (2012): Estimation of the spatial rainfall distribution using inverse distance weighting (IDW) in the middle of Taiwan. In Paddy Water Environ 10 (3), pp. 209–222. DOI: 10.1007/s10333-012-0319-1.

Chételat, John; McKinney, Melissa A.; Amyot, Marc; Dastoor, Ashu; Douglas, Thomas A.; Heimbürger-Boavida, Lars-Eric et al. (2022): Climate change and mercury in the Arctic: Abiotic interactions. In The Science of the total environment 824, p. 153715. DOI: 10.1016/j.scitotenv.2022.153715.

Coffin, Richard; Smith, Joseph; Yoza, Brandon; Boyd, Thomas; Montgomery, Michael (2017): Spatial Variation in Sediment Organic Carbon Distribution across the Alaskan Beaufort Sea Shelf. In Energies 10 (9), p. 1265. DOI: 10.3390/en10091265.

Couture, Nicole J.; Irrgang, Anna; Pollard, Wayne; Lantuit, Hugues; Fritz, Michael (2018): Coastal Erosion of Permafrost Soils Along the Yukon Coastal Plain and Fluxes of Organic Carbon to the Canadian Beaufort Sea. In J. Geophys. Res. Biogeosci. 123 (2), pp. 406–422. DOI: 10.1002/2017JG004166.

Cray, Heather A.; Pollard, Wayne H. (2015): Vegetation Recovery Patterns Following Permafrost Disturbance in a Low Arctic Setting: Case Study of Herschel Island, Yukon, Canada. In Arctic, Antarctic, and Alpine Research 47 (1), pp. 99–113. DOI: 10.1657/AAAR0013-076.

Dallimore, Scott R.; Wolfe, Stephen A.; Solomon, Steven M. (1996): Influence of ground ice and permafrost on coastal evolution, Richards Island, Beaufort Sea coast, N.W.T. In Can. J. Earth Sci. 33 (5), pp. 664–675. DOI: 10.1139/e96-050.

Dastoor, Ashu; Angot, Hélène; Bieser, Johannes; Christensen, Jesper H.; Douglas, Thomas A.; Heimbürger-Boavida, Lars-Eric et al. (2022): Arctic mercury cycling. In Nat Rev Earth Environ 3 (4), pp. 270–286. DOI: 10.1038/s43017-022-00269-w.

Deschamps, Charles-Edouard; Montero-Serrano, Jean-Carlos; St-Onge, Guillaume (2018): Sediment Provenance Changes in the Western Arctic Ocean in Response to Ice Rafting, Sea Level, and Oceanic Circulation Variations Since the Last Deglaciation.

In Geochem. Geophys. Geosyst. 19 (7), pp. 2147–2165. DOI: 10.1029/2017GC007411.

Dietz, Rune; Sonne, Christian; Basu, Niladri; Braune, Birgit; O'Hara, Todd; Letcher, Robert J. et al. (2013): What are the toxicological effects of mercury in Arctic biota? In The Science of the total environment 443, pp. 775–790. DOI: 10.1016/j.scitotenv.2012.11.046.

Dmitrenko, Igor A.; Kirillov, Sergei A.; Forest, Alexandre; Gratton, Yves; Volkov, Denis L.; Williams, William J. et al. (2016): Shelfbreak current over the Canadian Beaufort Sea con-tinental slope: Wind-driven events in January 2005. In J. Geophys. Res. Oceans 121 (4), pp. 2447–2468. DOI: 10.1002/2015JC011514.

Doxaran, D.; Devred, E.; Babin, M. (2015): A 50 % increase in the mass of terrestrial particles delivered by the Mackenzie River into the Beaufort Sea (Canadian Arctic Ocean) over the last 10 years. In Biogeosciences 12 (11), pp. 3551–3565. DOI: 10.5194/bg-12-3551-2015.

Doxaran, D.; Ehn, J.; Bélanger, S.; Matsuoka, A.; Hooker, S.; Babin, M. (2012): Optical characterisation of suspended particles in the Mackenzie River plume (Canadian Arctic Ocean) and implications for ocean colour remote sensing. In Biogeosciences 9 (8), pp. 3213–3229. DOI: 10.5194/bg-9-3213-2012.

Drenzek, Nicholas J.; Montluçon, Daniel B.; Yunker, Mark B.; Macdonald, Robie W.; Eglinton, Timothy I. (2007): Constraints on the origin of sedimentary organic carbon in the Beaufort Sea from coupled molecular 13C and 14C measurements. In Marine Chemistry 103 (1-2), pp. 146–162. DOI: 10.1016/j.marchem.2006.06.017.

Driscoll, Charles T.; Mason, Robert P.; Chan, Hing Man; Jacob, Daniel J.; Pirrone, Nicola (2013): Mercury as a global pollutant: sources, pathways, and effects. In Environmental science & technology 47 (10), pp. 4967–4983. DOI: 10.1021/es305071v.

Dunton, Kenneth H.; Weingartner, Thomas; Carmack, Eddy C. (2006): The nearshore western Beaufort Sea ecosystem: Circulation and importance of terrestrial carbon in arctic coastal food webs. In Progress in Oceanography 71 (2-4), pp. 362–378. DOI: 10.1016/j.pocean.2006.09.011.

Eicken, H.; Gradinger, R.; Gaylord, A.; Mahoney, A.; Rigor, I.; Melling, H. (2005): Sediment transport by sea ice in the Chukchi and Beaufort Seas: Increasing importance due to changing ice conditions? In Deep Sea Research Part II: Topical Studies in Oceanography 52 (24-26), pp. 3281–3302. DOI: 10.1016/j.dsr2.2005.10.006.

Elberling, Bo; Michelsen, Anders; Schädel, Christina; Schuur, Edward A. G.; Christiansen, Hanne H.; Berg, Louise et al. (2013): Long-term CO2 production following permafrost thaw. In Nature Clim Change 3 (10), pp. 890–894. DOI: 10.1038/nclimate1955.

Emmerton, Craig A.; Lesack, Lance F. W.; Marsh, Philip (2007): Lake abundance, potential water storage, and habitat distribution in the Mackenzie River Delta, western Canadian Arctic. In Water Resour. Res. 43 (5). DOI: 10.1029/2006WR005139.

Environmental Systems Research Institute (2022), available at: https://www.esri.com

Faust, Johan C.; Ascough, Philippa; Hilton, Robert G.; Stevenson, Mark A.; Hendry, Katharine R.; März, Christian (2023): New evidence for preservation of contemporary ma-rine organic carbon by iron in Arctic shelf sediments. In Environ. Res. Lett. 18 (1), p. 14006. DOI: 10.1088/1748-9326/aca780.

Fitzgerald, William F.; Lamborg, Carl H.; Hammerschmidt, Chad R. (2007): Marine biogeochemical cycling of mercury. In Chemical reviews 107 (2), pp. 641–662. DOI: 10.1021/cr050353m.

Forest, Alexandre; Osborne, Philip D.; Curtiss, Gregory; Lowings, Malcolm G. (2016): Current surges and seabed erosion near the shelf break in the Canadian Beaufort Sea: A response to wind and ice motion stress. In Journal of Marine Systems 160, pp. 1–16. DOI: 10.1016/j.jmarsys.2016.03.008.

Forest, Alexandre; Sampei, Makoto; Hattori, Hiroshi; Makabe, Ryosuke; Sasaki, Hiroshi; Fukuchi, Mitsuo et al. (2007): Particulate organic carbon fluxes on the slope of the Mackenzie Shelf (Beaufort Sea): Physical and biological forcing of shelf-basin exchanges. In Journal of Marine Systems 68 (1-2), pp. 39–54. DOI: 10.1016/j.jmarsys.2006.10.008.

Fox, Austin L.; Hughes, Emily A.; Trocine, Robert P.; Trefry, John H.; Schonberg, Susan V.; McTigue, Nathan D. et al. (2014): Mercury in the northeastern Chukchi Sea: Distribu-tion patterns in seawater and sediments and biomagnification in the benthic food web. In Deep Sea Research Part II: Topical Studies in Oceanography 102, pp. 56–67. DOI: 10.1016/j.dsr2.2013.07.012.

Fritz, Michael; Vonk, Jorien E.; Lantuit, Hugues (2017): Collapsing Arctic coastlines. In Nature Clim Change 7 (1), pp. 6–7. DOI: 10.1038/nclimate3188.

Goñi, Miguel A.; O'Connor, Alison E.; Kuzyk, Zou Zou; Yunker, Mark B.; Gobeil, Charles; Macdonald, Robie W. (2013): Distribution and sources of organic matter in surface marine sediments across the North American Arctic margin. In J. Geophys. Res. Oceans 118 (9), pp. 4017–4035. DOI: 10.1002/jgrc.20286.

Goñi, Miguel A.; Yunker, Mark B.; Macdonald, Robie W.; Eglinton, Timothy I. (2005): The supply and preservation of ancient and modern components of organic carbon in the Ca-nadian Beaufort Shelf of the Arctic Ocean. In Marine Chemistry 93 (1), pp. 53–73. DOI: 10.1016/j.marchem.2004.08.001.

Grotheer, H.; Meyer, V.; Riedel, T.; Pfalz, G.; Mathieu, L.; Hefter, J. et al. (2020): Burial and Origin of Permafrost-Derived Carbon in the Nearshore Zone of the Southern Canadi-an Beaufort Sea. In Geophys. Res. Lett. 47 (3). DOI: 10.1029/2019GL085897.

Günther, F.; Overduin, P. P.; Sandakov, A. V.; Grosse, G.; Grigoriev, M. N. (2013): Short- and long-term thermo-erosion of ice-rich permafrost coasts in the Laptev Sea region. In Biogeosciences 10 (6), pp. 4297–4318. DOI: 10.5194/bg-10-4297-2013.

Hanna, Andrea J.M.; Allison, Mead A.; Bianchi, Thomas S.; Marcantonio, Franco; Goff, John A. (2014): Late Holocene sedimentation in a high Arctic coastal setting: Simpson Lagoon and Colville Delta, Alaska. In Continental Shelf Research 74, pp. 11–24. DOI: 10.1016/j.csr.2013.11.026.

Hare, Alexander; Stern, Gary A.; Macdonald, Robie W.; Kuzyk, Zou Zou; Wang, Feiyue (2008): Contemporary and preindustrial mass budgets of mercury in the Hudson Bay Ma-rine System: the role of sediment recycling. In The Science of the total environment 406 (1-2), pp. 190–204. DOI: 10.1016/j.scitotenv.2008.07.033.

Harper. J.R., Penland. P.S. (1982): Beaufort Sea sediment dynamics. Contract Report to Atlantic Geoscience Centre. Geological Survey of Canada.

Hedges, John I.; Keil, Richard G. (1995): Sedimentary organic matter preservation: an assessment and speculative synthesis. In Marine Chemistry 49 (2-3), pp. 81–115. DOI: 10.1016/0304-4203(95)00008-F.

Héquette, A., Desrosiers, M., Hill, P.R., Forbes, D.L., (2001): The influence of coastal morphology on shoreface sediment transport under storm-combined flows, Canadian Beaufort Sea. J. In *Coast. Res.* (17), p. 507–516.

Hill, P. R.; Nadea, O. C. (1989): Storm-dominated Sedimentation on the Inner Shelf of the Canadian Beaufort Sea. In SEPM JSR Vol. 59. DOI: 10.1306/212F8FC1-2B24-11D7-8648000102C1865D.

Hill, Philip R.; Blasco, Steve M.; Harper, John R.; Fissel, David B. (1991): Sedimentation on the Canadian Beaufort Shelf. In Continental Shelf Research 11 (8-10), pp. 821–842. DOI: 10.1016/0278-4343(91)90081-G.

Hilton, Robert G.; Galy, Valier; Gaillardet, Jérôme; Dellinger, Mathieu; Bryant, Charlotte; O'Regan, Matt et al. (2015): Erosion of organic carbon in the Arctic as a geological carbon dioxide sink. In Nature 524 (7563), pp. 84–87. DOI: 10.1038/nature14653.

Hollesen, Jørgen; Matthiesen, Henning; Møller, Anders Bjørn; Elberling, Bo (2015): Permafrost thawing in organic Arctic soils accelerated by ground heat production. In Nature Clim Change 5 (6), pp. 574–578. DOI: 10.1038/nclimate2590.

Hoque, Md. Azharul; Pollard, Wayne H. (2009): Arctic coastal retreat through block failure. In Can. Geotech. J. 46 (10), pp. 1103–1115. DOI: 10.1139/T09-058.

Hugelius, G.; Strauss, J.; Zubrzycki, S.; Harden, J. W.; Schuur, E. A. G.; Ping, C.-L. et al. (2014): Estimated stocks of circumpolar permafrost carbon with quantified uncertainty ranges and identified data gaps. In Biogeosciences 11 (23), pp. 6573–6593. DOI: 10.5194/bg-11-6573-2014.

Irrgang, Anna M.; Bendixen, Mette; Farquharson, Louise M.; Baranskaya, Alisa V.; Erikson, Li H.; Gibbs, Ann E. et al. (2022): Drivers, dynamics and impacts of changing Arctic coasts. In Nat Rev Earth Environ 3 (1), pp. 39–54. DOI: 10.1038/s43017-021-00232-1.

Irrgang, Anna M.; Lantuit, Hugues; Manson, Gavin K.; Günther, Frank; Grosse, Guido; Overduin, Pier Paul (2018): Variability in Rates of Coastal Change Along the Yukon Coast, 1951 to 2015. In J. Geophys. Res. Earth Surf. 123 (4), pp. 779–800. DOI: 10.1002/2017JF004326.

Jones, Benjamin M.; Farquharson, Louise M.; Baughman, Carson A.; Buzard, Richard M.; Arp, Christopher D.; Grosse, Guido et al. (2018): A decade of remotely sensed observations highlight complex processes linked to coastal permafrost bluff erosion in the Arctic. In Environ. Res. Lett. 13 (11), p. 115001. DOI: 10.1088/1748-9326/aae471.

Karlsson, E. S.; Brüchert, V.; Tesi, T.; Charkin, A.; Dudarev, O.; Semiletov, I.; Gustafsson, Ö. (2015): Contrasting regimes for organic matter degradation in the East Siberian Sea and the Laptev Sea assessed through microbial incubations and molecular markers. In Marine Chemistry 170, pp. 11–22. DOI: 10.1016/j.marchem.2014.12.005.

Keil, Richard G.; Dickens, Angela F.; Arnarson, Thorarinn; Nunn, Brook L.; Devol, Allan H. (2004): What is the oxygen exposure time of laterally transported organic matter along the Washington margin? In Marine Chemistry 92 (1-4), pp. 157–165. DOI: 10.1016/j.marchem.2004.06.024.

Kim, Dahae; Kim, Jung-Hyun; Tesi, Tommaso; Kang, Sujin; Nogarotto, Alessio; Park, Kwangkyu et al. (2022): Changes in the burial efficiency and composition of terrestrial organic carbon along the Mackenzie Trough in the Beaufort Sea. In Estuarine, Coastal and Shelf Science 275, p. 107997. DOI: 10.1016/j.ecss.2022.107997.

Kim, J.-H.; Peterse, F.; Willmott, V.; Kristensen, D. Klitgaard; Baas, M.; Schouten, S.; Sinninghe Damsté, J. S. (2011): Large ancient organic matter contributions to Arctic marine sediments (Svalbard). In Limnol. Oceanogr. 56 (4), pp. 1463–1474. DOI: 10.4319/lo.2011.56.4.1463.

Knies, Jochen; Brookes, Steven; Schubert, Carsten J. (2007): Re-assessing the nitrogen signal in continental margin sediments: New insights from the high northern latitudes. In Earth and Planetary Science Letters 253 (3-4), pp. 471–484. DOI: 10.1016/j.epsl.2006.11.008.

Knoblauch, Christian; Beer, Christian; Sosnin, Alexander; Wagner, Dirk; Pfeiffer, Eva-Maria (2013): Predicting long-term carbon mineralization and trace gas production from

thawing permafrost of Northeast Siberia. In Global change biology 19 (4), pp. 1160–1172. DOI: 10.1111/gcb.12116.

Kohler, Stephen G.; Kull, Laura M.; Heimbürger-Boavida, Lars-Eric; Ricardo de Freitas, Thaise; Sanchez, Nicolas; Ndungu, Kuria; Ardelan, Murat V. (2022): Distribution pattern of mercury in northern Barents Sea and Eurasian Basin surface sediment. In Marine pollu-tion bulletin 185 (Pt A), p. 114272. DOI: 10.1016/j.marpolbul.2022.114272.

Koven, Charles D.; Riley, William J.; Stern, Alex (2013): Analysis of Permafrost Thermal Dynamics and Response to Climate Change in the CMIP5 Earth System Models. In Jour-nal of Climate 26 (6), pp. 1877–1900. DOI: 10.1175/JCLI-D-12-00228.1.

Lalande, Catherine; Forest, Alexandre; Barber, David G.; Gratton, Yves; Fortier, Louis (2009): Variability in the annual cycle of vertical particulate organic carbon export on Arctic shelves: Contrasting the Laptev Sea, Northern Baffin Bay and the Beaufort Sea. In Conti-nental Shelf Research 29 (17), pp. 2157–2165. DOI: 10.1016/j.csr.2009.08.009.

Lam, Nina Siu-Ngan (1983): Spatial Interpolation Methods: A Review. In The American Cartographer 10 (2), pp. 129–150. DOI: 10.1559/152304083783914958.

Lamb, Angela L.; Wilson, Graham P.; Leng, Melanie J. (2006): A review of coastal palaeoclimate and relative sea-level reconstructions using δ13C and C/N ratios in organic mate-rial. In Earth-Science Reviews 75 (1-4), pp. 29–57. DOI: 10.1016/j.earscirev.2005.10.003.

Lancianese, Valerio; Dinelli, Enrico (2015): Different spatial methods in regional geochemical mapping at high density sampling: An application on stream sediment of Romagna Apennines, Northern Italy. In Journal of Geochemical Exploration 154, pp. 143–155. DOI: 10.1016/j.gexplo.2014.12.014.

Lantuit, H.; Pollard, W. H. (2008): Fifty years of coastal erosion and retrogressive thaw slump activity on Herschel Island, southern Beaufort Sea, Yukon Territory, Canada. In Geomorphology 95 (1-2), pp. 84–102. DOI: 10.1016/j.geomorph.2006.07.040.

Lantuit, Hugues; Overduin, Pier Paul; Couture, Nicole; Wetterich, Sebastian; Aré, Felix; Atkinson, David et al. (2012): The Arctic Coastal Dynamics Database: A New Classification Scheme and Statistics on Arctic Permafrost Coastlines. In Estuaries and Coasts 35 (2), pp. 383–400. DOI: 10.1007/s12237-010-9362-6.

Leitch, Daniel R.; Carrie, Jesse; Lean, David; Macdonald, Robie W.; Stern, Gary A.; Wang, Feiyue (2007): The delivery of mercury to the Beaufort Sea of the Arctic Ocean by the Mackenzie River. In The Science of the total environment 373 (1), pp. 178–195. DOI: 10.1016/j.scitotenv.2006.10.041.

Lesack, Lance F. W.; Marsh, Philip; Hicks, Faye E.; Forbes, Donald L. (2013): Timing, duration, and magnitude of peak annual water-levels during ice breakup in the Mackenzie Delta and the role of river discharge. In Water Resour. Res. 49 (12), pp. 8234–8249. DOI: 10.1002/2012WR013198.

Letscher, Robert T.; Hansell, Dennis A.; Kadko, David (2011): Rapid removal of terrigenous dissolved organic carbon over the Eurasian shelves of the Arctic Ocean. In Marine Chemistry 123 (1-4), pp. 78–87. DOI: 10.1016/j.marchem.2010.10.002.

Letscher, Robert T.; Hansell, Dennis A.; Kadko, David; Bates, Nicholas R. (2013): Dissolved organic nitrogen dynamics in the Arctic Ocean. In Marine Chemistry 148, pp. 1–9. DOI: 10.1016/j.marchem.2012.10.002.

Lewis C.P. (1988): Mackenzie Delta sedimentary environments and processes. Unpublished contract report. Ottawa: Sediment Survey Section, Environment Canada.

Lewkowicz, A.G. (1990): Morphology, Frequency and Magnitude of Active Layer Detachment Slides, Fosheim Peninsula, Ellesmere Island, N.W.T. Final Proceedings, Fifth Canadian Permafrost Conference. Université Laval, Quebec City, pp. 111-118.

Li, Jin; Heap, Andrew D. (2011): A review of comparative studies of spatial interpolation methods in environmental sciences: Performance and impact factors. In Ecological Infor-matics 6 (3-4), pp. 228–241. DOI: 10.1016/j.ecoinf.2010.12.003.

Li, Zhanglin (2021): An enhanced dual IDW method for high-quality geospatial interpolation. In Scientific reports 11 (1), p. 9903. DOI: 10.1038/s41598-021-89172-w.

Linick, Timothy W. (1980): Bomb-Produced Carbon-14 in the Surface Water of the Pacific Ocean. In Radiocarbon 22 (3), pp. 599–606. DOI: 10.1017/S0033822200009978.

Lintern, D. Gwyn; Macdonald, Robie W.; Solomon, Steven M.; Jakes, Hunter (2013): Beaufort Sea storm and resuspension modeling. In Journal of Marine Systems 127, pp. 14–25. DOI: 10.1016/j.jmarsys.2011.11.015.

Macdonald, R. W. (2000): Arctic Estuaries and Ice: A Positive—Negative Estuarine Couple. In Edward Lyn Lewis, E. Peter Jones, Peter Lemke, Terry D. Prowse, Peter Wadhams (Eds.): The Freshwater Budget of the Arctic Ocean. Dordrecht: Springer Netherlands, pp. 383–407.

Macdonald, R. W.; Solomon, S. M.; Cranston, R. E.; Welch, H. E.; Yunker, M. B.; Gobeil, C. (1998): A sediment and organic carbon budget for the Canadian Beaufort Shelf. In Ma-rine Geology 144 (4), pp. 255–273. DOI: 10.1016/S0025-3227(97)00106-0.

Magen, Cédric; Chaillou, Gwénaëlle; Crowe, Sean A.; Mucci, Alfonso; Sundby, Bjørn; Gao, Aiguo et al. (2010): Origin and fate of particulate organic matter in the southern Beaufort Sea – Amundsen Gulf region, Canadian Arctic. In Estuarine, Coastal and Shelf Science 86 (1), pp. 31–41. DOI: 10.1016/j.ecss.2009.09.009.

Maslanik, James; Stroeve, Julienne; Fowler, Charles; Emery, William (2011): Distribution and trends in Arctic sea ice age through spring 2011. In Geophys. Res. Lett. 38 (13), n/a-n/a. DOI: 10.1029/2011GL047735.

McClelland, J. W.; Holmes, R. M.; Peterson, B. J.; Raymond, P. A.; Striegl, R. G.; Zhulidov, A. V. et al. (2016): Particulate organic carbon and nitrogen export from major Arctic rivers. In Global Biogeochem. Cycles 30 (5), pp. 629–643. DOI: 10.1002/2015GB005351.

Meier, Walter N.; Hovelsrud, Greta K.; van Oort, Bob E.H.; Key, Jeffrey R.; Kovacs, Kit M.; Michel, Christine et al. (2014): Arctic sea ice in transformation: A review of recent observed changes and impacts on biology and human activity. In Rev. Geophys. 52 (3), pp. 185–217. DOI: 10.1002/2013RG000431.

Mu, Cuicui; Zhang, Feng; Chen, Xu; Ge, Shemin; Mu, Mei; Jia, Lin et al. (2019): Carbon and mercury export from the Arctic rivers and response to permafrost degradation. In Wa-ter research 161, pp. 54–60. DOI: 10.1016/j.watres.2019.05.082.

Müller, P.J (1977): CN ratios in Pacific deep-sea sediments: Effect of inorganic ammonium and organic nitrogen compounds sorbed by clays. In Geochimica et Cosmochimica Acta 41 (6), pp. 765–776. DOI: 10.1016/0016-7037(77)90047-3.

Mulligan, Ryan P.; Perrie, Will; Solomon, Steve (2010): Dynamics of the Mackenzie River plume on the inner Beaufort shelf during an open water period in summer. In Estuarine, Coastal and Shelf Science 89 (3), pp. 214–220. DOI: 10.1016/j.ecss.2010.06.010.

Murdoch D, Adler D (2023). *rgl: 3D Visualization Using OpenGL*. https://github.com/dmurdoch/rgl, https://dmurdoch.github.io/rgl/.

Mustapha, Sélima Ben; Larouche, Pierre; Dubois, Jean-Marie (2016): Spatial and temporal variability of sea-surface temperature fronts in the coastal Beaufort Sea. In Continen-tal Shelf Research 124, pp. 134–141. DOI: 10.1016/j.csr.2016.06.001.

Naidu, A. S.; Cooper, L. W.; Finney, B. P.; Macdonald, R. W.; Alexander, C.; Semiletov, I. P. (2000): Organic carbon isotope ratios (δ 13 C) of Arctic Amerasian Continental shelf sediments. In International Journal of Earth Sciences 89 (3), pp. 522–532. DOI: 10.1007/s005310000121.

National Snow an Ice Data Center (2022), available at: http://nsidc.org

Nikolopoulos, Anna; Pickart, Robert S.; Fratantoni, Paula S.; Shimada, Koji; Torres, Daniel J.; Jones, E. Peter (2009): The western Arctic boundary current at 152°W: Structure, variability, and transport. In Deep Sea Research Part II: Topical Studies in Oceanography 56 (17), pp. 1164–1181. DOI: 10.1016/j.dsr2.2008.10.014.

O'Brien, M. C.; Macdonald, R. W.; Melling, H.; Iseki, K. (2006): Particle fluxes and geochemistry on the Canadian Beaufort Shelf: Implications for sediment transport and deposi-tion. In Continental Shelf Research 26 (1), pp. 41–81. DOI: 10.1016/j.csr.2005.09.007.

O'Brien, Mary C.; Melling, Humfrey; Pedersen, Thomas F.; Macdonald, Robie W. (2013): The role of eddies on particle flux in the Canada Basin of the Arctic Ocean. In Deep Sea Research Part I: Oceanographic Research Papers 71, pp. 1–20. DOI: 10.1016/j.dsr.2012.10.004.

Obrist, Daniel (2007): Atmospheric mercury pollution due to losses of terrestrial carbon pools? In Biogeochemistry 85 (2), pp. 119–123. DOI: 10.1007/s10533-007-9108-0.

Osborne, Philip D.; Forest, Alexandre (2016): Sediment Dynamics from Coast to Slope – Southern Canadian Beaufort Sea. In Journal of Coastal Research 75 (sp1), pp. 537–541. DOI: 10.2112/SI75-108.1.

Outridge, P. M.; Macdonald, R. W.; Wang, F.; Stern, G. A.; Dastoor, A. P. (2008): A mass balance inventory of mercury in the Arctic Ocean. In Environ. Chem. 5 (2), p. 89. DOI: 10.1071/EN08002.

Overland, James E. (2009): Meteorology of the Beaufort Sea. In J. Geophys. Res. 114. DOI: 10.1029/2008JC004861.

Rachold, V.; Eicken, H.; Gordeev, V. V.; Grigoriev, M. N.; Hubberten, H.-W.; Lisitzin, A. P. et al. (2004): Modern Terrigenous Organic Carbon Input to the Arctic Ocean. In Ruediger Stein, Robie W. Macdonald (Eds.): The Organic Carbon Cycle in the Arctic Ocean. Berlin, Heidelberg: Springer Berlin Heidelberg, pp. 33–55.

Rachold, Volker; Grigoriev, Mikhail N.; Are, Felix E.; Solomon, Steve; Reimnitz, Erk; Kassens, Heidemarie; Antonow, Martin (2000): Coastal erosion vs riverine sediment discharge in the Arctic Shelf seas. In International Journal of Earth Sciences 89 (3), pp. 450–460. DOI: 10.1007/s005310000113.

Radosavljevic, Boris; Lantuit, Hugues; Knoblauch, Christian; Couture, Nicole; Herzschuh, Ulrike; Fritz, Michael (2022): Arctic Nearshore Sediment Dynamics—An Example from Herschel Island—Qikiqtaruk, Canada. In JMSE 10 (11), p. 1589. DOI: 10.3390/jmse10111589.

Redfield, Alfred Clarence (1934): On the proportions of organic derivatives in sea water and their relation to the composition of plankton. In *James Johnstone memorial*, pp. 176-192.

Redfield, A., Ketchum, B. and Richards, F., (1963) The Influence of Organisms on the Composition of Seawater. In: Hill, M.N., Ed., The Sea, Vol. 2, The Composition of Sea-

Water Comparative and Descriptive Oceanography, Interscience Publishers, New York, 26-77.

Richerol, Thomas; Rochon, André; Blasco, Steve; Scott, Dave B.; Schell, Trecia M.; Bennett, Robbie J. (2008): Distribution of dinoflagellate cysts in surface sediments of the Mac-kenzie Shelf and Amundsen Gulf, Beaufort Sea (Canada). In Journal of Marine Systems 74 (3-4), pp. 825–839. DOI: 10.1016/j.jmarsys.2007.11.003.

Rood, Stewart B.; Kaluthota, Sobadini; Philipsen, Laurens J.; Rood, Neil J.; Zanewich, Karen P. (2017): Increasing discharge from the Mackenzie River system to the Arctic Ocean. In Hydrol. Process. 31 (1), pp. 150–160. DOI: 10.1002/hyp.10986.

Ruttenberg, K. C.; Goñi, M. A. (1997): Phosphorus distribution, C:N:P ratios, and δ13Coc in arctic, temperate, and tropical coastal sediments: tools for characterizing bulk sedimen-tary organic matter. In Marine Geology 139 (1-4), pp. 123–145. DOI: 10.1016/S0025-3227(96)00107-7.

Sanei, Hamed; Outridge, Peter M.; Oguri, Kazumasa; Stern, Gary A.; Thamdrup, Bo; Wenzhöfer, Frank et al. (2021): High mercury accumulation in deep-ocean hadal sediments. In Scientific reports 11 (1), p. 10970. DOI: 10.1038/s41598-021-90459-1.

Schubert, Carsten J.; Calvert, Stephen E. (2001): Nitrogen and carbon isotopic composition of marine and terrestrial organic matter in Arctic Ocean sediments. In Deep Sea Re-search Part I: Oceanographic Research Papers 48 (3), pp. 789–810. DOI: 10.1016/S0967-0637(00)00069-8.

Schuster, Paul F.; Schaefer, Kevin M.; Aiken, George R.; Antweiler, Ronald C.; Dewild, John F.; Gryziec, Joshua D. et al. (2018): Permafrost Stores a Globally Significant Amount of Mercury. In Geophys. Res. Lett. 45 (3), pp. 1463–1471. DOI: 10.1002/2017GL075571.

Schuur, E. A. G.; McGuire, A. D.; Schädel, C.; Grosse, G.; Harden, J. W.; Hayes, D. J. et al. (2015): Climate change and the permafrost carbon feedback. In Nature 520 (7546), pp. 171–179. DOI: 10.1038/nature14338.

Semiletov, I. P.; Pipko, I. I.; Shakhova, N. E.; Dudarev, O. V.; Pugach, S. P.; Charkin, A. N. et al. (2011): Carbon transport by the Lena River from its headwaters to the Arctic Ocean, with emphasis on fluvial input of terrestrial particulate organic carbon vs. carbon transport by coastal erosion. In Biogeosciences 8 (9), pp. 2407–2426. DOI: 10.5194/bg-8-2407-2011.

Serreze, Mark C.; Barrett, Andrew P.; Slater, Andrew G.; Woodgate, Rebecca A.; Aagaard, Knut; Lammers, Richard B. et al. (2006): The large-scale freshwater cycle of the Arctic. In J. Geophys. Res. 111 (C11). DOI: 10.1029/2005JC003424.

Smith, Walker O. (2010): Polar Margins. In Kon-Kee Liu, Larry Atkinson, Renato Quiñones, Liana Talaue-McManus (Eds.): Carbon and Nutrient Fluxes in Continental Margins. Berlin: Springer (Global Change - The IGBP Series), pp. 289–330.

Soerensen, Anne L.; Jacob, Daniel J.; Schartup, Amina T.; Fisher, Jenny A.; Lehnherr, Igor; St. Louis, Vincent L. et al. (2016): A mass budget for mercury and methylmercury in the Arctic Ocean. In Global Biogeochem. Cycles 30 (4), pp. 560–575. DOI: 10.1002/2015GB005280.

Sonke, Jeroen E.; Teisserenc, Roman; Heimbürger-Boavida, Lars-Eric; Petrova, Mariia V.; Marusczak, Nicolas; Le Dantec, Theo et al. (2018): Eurasian river spring flood obser-vations support net Arctic Ocean mercury export to the atmosphere and Atlantic Ocean. In Proceedings of the National Academy of Sciences of the United States of America 115 (50), E11586-E11594. DOI: 10.1073/pnas.1811957115.

Spadoni, Massimo (2006): Geochemical mapping using a geomorphologic approach based on catchments. In Journal of Geochemical Exploration 90 (3), pp. 183–196. DOI: 10.1016/j.gexplo.2005.12.001.

Stern, Gary A.; Macdonald, Robie W.; Outridge, Peter M.; Wilson, Simon; Chételat, John; Cole, Amanda et al. (2012): How does climate change influence Arctic mercury? In The Science of the total environment 414, pp. 22–42. DOI: 10.1016/j.scitotenv.2011.10.039.

Stevenson, F. J. (1994): Humus chemistry. Genesis, composition, reactions. 2nd ed. New York, N.Y.: Wiley.

Strauss, Jens; Schirrmeister, Lutz; Grosse, Guido; Fortier, Daniel; Hugelius, Gustaf; Knoblauch, Christian et al. (2017): Deep Yedoma permafrost: A synthesis of depositional characteristics and carbon vulnerability. In Earth-Science Reviews 172, pp. 75–86. DOI: 10.1016/j.earscirev.2017.07.007.

Streets, David G.; Devane, Molly K.; Lu, Zifeng; Bond, Tami C.; Sunderland, Elsie M.; Jacob, Daniel J. (2011): All-time releases of mercury to the atmosphere from human ac-tivities. In Environmental science & technology 45 (24), pp. 10485–10491. DOI: 10.1021/es202765m.

Stroeve, J. C.; Markus, T.; Boisvert, L.; Miller, J.; Barrett, A. (2014): Changes in Arctic melt season and implications for sea ice loss. In Geophys. Res. Lett. 41 (4), pp. 1216–1225. DOI: 10.1002/2013GL058951.

Tanski, G.; Wagner, D.; Knoblauch, C.; Fritz, M.; Sachs, T.; Lantuit, H. (2019): Rapid CO 2 Release From Eroding Permafrost in Seawater. In Geophys. Res. Lett. 46 (20), pp. 11244–11252. DOI: 10.1029/2019GL084303.

Tanski, George; Bröder, Lisa; Wagner, Dirk; Knoblauch, Christian; Lantuit, Hugues; Beer, Christian et al. (2021): Permafrost Carbon and CO2 Pathways Differ at Contrasting Coastal Erosion Sites in the Canadian Arctic. In Front. Earth Sci. 9, Article 630493. DOI: 10.3389/feart.2021.630493.

Tanski, George; Lantuit, Hugues; Ruttor, Saskia; Knoblauch, Christian; Radosavljevic, Boris; Strauss, Jens et al. (2017): Transformation of terrestrial organic matter along thermokarst-affected permafrost coasts in the Arctic. In The Science of the total environment 581-582, pp. 434–447. DOI: 10.1016/j.scitotenv.2016.12.152.

Tatsii, Yu. G.; Baranov, D. Yu. (2022): Features of Mercury Accumulation in the Bottom Sediments of Two Arctic Lakes in West Siberia. In Geochem. Int. 60 (2), pp. 213–221. DOI: 10.1134/S0016702922020094.

Vonk, J. E.; Sánchez-García, L.; van Dongen, B. E.; Alling, V.; Kosmach, D.; Charkin, A. et al. (2012): Activation of old carbon by erosion of coastal and subsea permafrost in Arc-tic Siberia. In Nature 489 (7414), pp. 137–140. DOI: 10.1038/nature11392.

Vonk, Jorien E.; Giosan, Liviu; Blusztajn, Jerzy; Montlucon, Daniel; Graf Pannatier, Elisabeth; McIntyre, Cameron et al. (2015): Spatial variations in geochemical characteristics of the modern Mackenzie Delta sedimentary system. In Geochimica et Cosmochimica Acta 171, pp. 100–120. DOI: 10.1016/j.gca.2015.08.005.

Vonk, Jorien E.; Mann, Paul J.; Davydov, Sergey; Davydova, Anna; Spencer, Robert G. M.; Schade, John et al. (2013): High biolability of ancient permafrost carbon upon thaw. In Geophys. Res. Lett. 40 (11), pp. 2689–2693. DOI: 10.1002/grl.50348.

Vonk, Jorien E.; Semiletov, Igor P.; Dudarev, Oleg V.; Eglinton, Timothy I.; Andersson, August; Shakhova, Natalia et al. (2014): Preferential burial of permafrost-derived organic carbon in Siberian-Arctic shelf waters. In J. Geophys. Res. Oceans 119 (12), pp. 8410–8421. DOI: 10.1002/2014JC010261.

Walker, Tony R. (2016): Mercury concentrations in marine sediments near a former mercury cell chlor-alkali plant in eastern Canada. In Marine pollution bulletin 107 (1), pp. 398–401. DOI: 10.1016/j.marpolbul.2016.03.033.

Wegner, Carolyn; Bennett, Katrina E.; Vernal, Anne de; Forwick, Matthias; Fritz, Michael; Heikkilä, Maija et al. (2015): Variability in transport of terrigenous material on the shelves and the deep Arctic Ocean during the Holocene. In Polar Research 34 (1), p. 24964. DOI: 10.3402/polar.v34.24964.

Wickham H (2007). “Reshaping Data with the reshape Package.” *Journal of Statistical Software*, **21**(12), 1–20. http://www.jstatsoft.org/v21/i12/.

Winkelmann, Daniel; Knies, Jochen (2005): Recent distribution and accumulation of organic carbon on the continental margin west off Spitsbergen. In Geochem. Geophys. Ge-osyst. 6 (9), n/a-n/a. DOI: 10.1029/2005GC000916.

Yunker, Mark B.; Macdonald, Robie W.; Snowdon, Lloyd R.; Fowler, Brian R. (2011): Alkane and PAH biomarkers as tracers of terrigenous organic carbon in Arctic Ocean sedi-ments. In Organic Geochemistry. DOI: 10.1016/j.orggeochem.2011.06.007.

Appendix

Please find the R-codes of the figures (Fig. 2, 17, 18/19) in the following GitHub-Folder:

https://github.com/Kathi2105/Masther-thesis-PeCaBeau2021

Tab. 1: PCB Stations in Spatial Relation

Station	Latitude (DD)	Longitude (DD)	Water Depth (m)	Distance to Delta (km)	Distance to Coast (km)
PCB01	71.2328753	-125.59845	411.4	493.7	155.6
PCB02	71.6219965	-128.10599	313.79	433.9	113.3
PCB03	72.1118265	-131.04685	1043.56	403.1	225.5
PCB04	71.4510997	-131.2942	531.11	336.4	145.8
PCB05	71.2029417	-131.35189	75.09	312.9	127.2
PCB06	70.7618287	-131.42986	50.01	279.8	78.9
PCB07	70.534833	-131.49528	52.03	265.3	55.7
PCB08	70.5217703	-133.62978	68.53	188.8	96.7
PCB09	71.1024253	-135.14449	675	224.9	156.4
PCB10	70.9095063	-136.28213	954.2	200.6	152.5
PCB11	70.5474777	-136.00952	74.4	159.7	110.7
PCB12	70.2798583	-135.77562	56.62	133.1	81.8
PCB13	69.9916265	-135.44577	32.09	56.7	49.5
PCB14	70.2387003	-137.18105	57.28	129.6	116.4
PCB16	70.5035005	-138.83108	795.13	180.6	107
PCB17	69.4270342	-138.02674	54.49	72.2	31.6
PCB17a	69.2878232	-137.27927	19.63	40	21.3
PCB18	69.9830043	-138.65143	267.12	132.2	41.5
PCB19	70.1660455	-138.90707	373.82	154.5	60.1
PCB20	70.5499128	-139.82038	783.13	209.3	109
PCB21	70.354771	-139.98316	457.67	195.1	86.2
PCB22	70.1227675	-140.24577	48	186.8	59.9
PCB23	69.8103258	-140.54852	33.18	180	22.8

Tab. 2: Sample List with Water Content

Station	Weight wet (g) with bag	Weight dry (g) with bag	Water Mass (g)	Gravimetric Water Content (%)	Dry Bulk Density (g/cm^3)	Volumetric Water Content (%)
PCB01_0-1cm	107.22	33.26	73.96	71.87	0.408	104.342
PCB01_1-2cm	76.02	27.01	49.01	68.347	0.32	69.143
PCB02_0-1cm	98.36	31.8	66.56	70.772	0.388	93.903
PCB02_1-2cm	135.3	51.24	84.06	64.174	0.662	11.591
PCB03_0-1cm	83.72	24.82	58.9	72.519	0.315	83.096
PCB03_1-2cm	79.74	27.63	52.11	67.465	0.355	73.517
PCB04_0-1cm	92.39	30.47	61.92	68.884	0.395	87.356
PCB04_1-2cm	84.72	30.97	53.75	65.373	0.402	75.83
PCB05_0-1cm	92.55	51.07	41.48	46.063	0.685	58.52
PCB05_1-2cm	97.91	53.93	43.98	46.096	0.726	62.047
PCB06_0-1cm	64.89	21.39	43.5	69.723	0.266	61.37
PCB06_1-2cm	76.14	28.94	47.2	64.096	0.373	66.59
PCB07_0-1cm	61.04	19.08	41.96	71.677	0.234	59.197
PCB07_1-2cm	74.92	26.37	48.55	67.039	0.337	68.494
PCB08_0-1cm	76	21.89	54.11	73.619	0.274	76.338
PCB08_1-2cm	79.13	26.81	52.32	68.276	0.343	73.813
PCB09_0-1cm	71.51	21.78	49.73	72.062	0.272	70.159
PCB09_1-2cm	79.47	27.73	51.74	67.221	0.356	72.995
PCB10_0-1cm	79.01	23.68	55.33	72.317	0.299	78.059
PCB10_1-2cm	85.11	30.24	54.87	66.421	0.391	77.41
PCB11_0-1cm	105.64	33.26	72.38	70.176	0.434	102.113
PCB11_1-2cm	86.92	32.87	54.05	64.025	0.428	76.253
PCB12_0-1cm	74.9	22.73	52.17	72.058	0.285	73.601
PCB12_1-2cm	57.19	20.16	37.03	67.709	0.249	52.242
PCB13_0-1cm	75.35	27.31	48.04	65.944	0.35	67.775
PCB13_1-2cm	74.76	30.85	43.91	60.767	0.4	61.948
PCB14_0-1cm	97.18	33.13	64.05	67.649	0.432	90.361
PCB14_1-2cm	85.49	33.68	51.81	62.429	0.44	73.093
PCB16_0-1cm	82.86	24.59	58.27	72.511	0.312	82.207
PCB16_1-2cm	102.05	36.16	65.89	66.188	0.475	92.957
PCB17_0-1cm	95.21	34.09	61.12	65.926	0.446	86.228
PCB17_1-2cm	82.11	33.62	48.49	60.909	0.439	68.409

PCB17a_0-1cm	68.49	38.57	29.92	45.34	0.509	42.211
PCB17a_1-2cm	100.79	59.25	41.54	42.263	0.801	58.604
PCB18_0-1cm	82.82	26.47	56.35	70.157	0.338	79.498
PCB18_1-2cm	83.25	32.37	50.88	63.009	0.421	71.781
PCB19_0-1cm	87.92	28.47	59.45	69.597	0.366	83.872
PCB19_1-2cm	85.31	31.99	53.32	64.388	0.416	75.224
PCB20_0-1cm	74.07	21.72	52.35	73.145	0.271	73.855
PCB20_1-2cm	74.92	25.99	48.93	67.564	0.331	69.03
PCB21_0-1cm	89	29.81	59.19	68.428	0.385	83.505
PCB21_1-2cm	89.37	35.4	53.97	62.127	0.464	76.141
PCB22_0-1cm	112.31	84.37	27.94	25.444	1.155	39.418
PCB22_1-2cm	118.83	79.43	39.4	33.869	1.085	55.585
PCB23_0-1cm	88.02	35.51	52.51	61.401	0.466	74.081
PCB23_1-2cm	90.86	46.24	44.62	50.498	0.617	62.95

Tab. 3: Sample List with Lab Results

Station	**TOC (%)**	**TN (%)**	**C/N ratio**	**$\Delta^{13}C$ (‰)**	**$\Delta^{15}N$ (‰)**	**Hg (µg/kg)**	**D50 Grain Size (µm)**	**^{14}C age yr**	**Age std. yr**	**Median ^{14}C Age Calib. BP**
PCB01_0-1cm	1.4	0.20	7.92	-23.9	7.18	103.37	3.94	5.383	82	5560
PCB01_1-2cm	1.4	0.20	8.16	-23.9	7.67	104.74	3.67	5.800	84	6018
PCB02_0-1cm	1.3	0.21	7.33	-24.1	6.93	101.86	3.96	6.494	87	6766
PCB02_1-2cm	1.3	0.21	7.36	-24.1	6.89	103.03	4.06	6.346	84	6595
PCB03_0-1cm	1.2	0.20	6.86	-23.8	7.02	104.85	3.00	7.336	91	7621
PCB03_1-2cm	1.1	0.19	7.14	-23.6	7.03	103.61	3.01	7.408	86	7690
PCB04_0-1cm	1.8	0.20	7.81	-24.8	6.43	98.55	3.68	8.680	96	9152
PCB04_1-2cm	1.3	0.21	7.31	-24.7	6.25	106.12	3.59	8.428	92	8810
PCB05_0-1cm	0.8	0.14	6.85	-24.6	7.32	51.92	50.18	6.226	85	6465
PCB05_1-2cm	0.8	0.14	6.76	-24.8	6.55	53.09	19.45	4.350	77	4294
PCB06_0-1cm	1.4	0.23	7.42	-25.0	6.59	80.32	5.87	5.931	85	6150
PCB06_1-2cm	1.4	0.23	6.97	-25.0	6.39	79.23	5.55	6.243	83	6483
PCB07_0-1cm	1.6	0.21	9.02	-25.1	5.90	84.75	4.51	6.178	85	6415
PCB07_1-2cm	1.6	0.26	7.44	-25.2	6.02	84.74	4.26	6.157	82	6392
PCB08_0-1cm	1.7	0.28	7.35	-25.1	6.88	92.76	3.85	6.747	88	7052
PCB08_1-2cm	1.6	0.26	7.21	-25.1	6.19	96.49	3.76	6.583	85	6868

PCB09_0-1cm	1.4	0.21	7.85	-24.8	6.48	102.52	3.22	7.654	92	7931
PCB09_1-2cm	1.4	0.22	7.34	-24.8	6.41	104.06	3.41	8.678	97	9150
PCB10_0-1cm	1.4	0.22	7.14	-24.8	6.66	110.84	3.32	7.810	92	8095
PCB10_1-2cm	1.4	0.21	7.60	-24.7	6.68	109.95	3.18	8.152	92	8464
PCB11_0-1cm	1.5	0.24	7.36	-25.4	5.69	99.92	3.76	7.765	94	8051
PCB11_1-2cm	1.4	0.19	8.46	-25.5	5.61	100.53	3.88	8.469	94	8863
PCB12_0-1cm	1.6	0.25	7.48	-25.7	6.16	96.84	3.32	6.554	87	6834
PCB12_1-2cm	1.6	0.23	7.80	-25.7	5.76	96.78	3.67	7.567	88	7842
PCB13_0-1cm	1.6	0.22	8.52	-26.1	5.48	88.36	3.76	8.905	98	9406
PCB13_1-2cm	1.5	0.20	8.71	-26.1	5.15	88.52	3.72	9.178	100	9748
PCB14_0-1cm	1.5	0.21	8.47	-25.8	5.42	90.08	3.62	8.577	97	9020
PCB14_1-2cm	1.5	0.17	9.98	-25.9	5.13	94.28	3.65	9.936	108	10794
PCB16_0-1cm	1.4	0.19	8.46	-24.7	6.81	109.72	2.97	7.622	90	7897
PCB16_1-2cm	1.3	0.21	7.08	-24.7	7.12	110.53	3.08	7.994	91	8284
PCB17_0-1cm	1.6	0.20	9.08	-25.8	5.50	91.48	3.96	8.544	100	8970
PCB17_1-2cm	1.5	0.18	9.70	-25.8	5.19	90.95	4.55	9.713	97	10459
PCB17a_0-1cm	1.4	0.14	11.71	-26.4	3.82	86.01	6.22	9.525	105	10223
PCB17a_1-2cm	1.4	0.14	11.35	-26.4	3.70	87.18	5.38	9.128	95	9682
PCB18_0-1cm	1.5	0.20	8.94	-25.1	6.58	104.98	3.74	7.344	90	7629
PCB18_1-2cm	1.4	0.19	8.43	-25.1	6.28	106.35	3.58	7.627	90	7902
PCB19_0-1cm	1.4	0.19	8.56	-25.0	6.56	108.73	3.87	6.920	89	7234
PCB19_1-2cm	1.4	0.20	8.06	-24.9	6.79	99.84	3.92	7.434	88	7715
PCB20_0-1cm	1.4	0.23	7.35	-24.6	7.23	106.25	3.08	7.326	92	7612
PCB20_1-2cm	1.4	0.20	8.10	-24.5	6.99	108.25	3.29	7.839	88	8124
PCB21_0-1cm	1.3	0.19	8.36	-24.6	6.41	103.71	4.06	7.257	90	7546
PCB21_1-2cm	1.2	0.19	7.59	-24.5	7.00	107.7	4.34	7.498	86	7775
PCB22_0-1cm	0.6	0.13	5.41	-25.0	7.86	36.06	71.88	6.990	89	7303
PCB22_1-2cm	0.6	0.10	7.50	-25.0	7.10	45.03	15.78	6.352	83	6601
PCB23_0-1cm	1.3	0.18	8.56	-25.1	6.51	63.89	8.74	7.845	97	8130
PCB23_1-2cm	1.1	0.13	10.06	-25.3	5.74	63.09	8.65	6.896	86	7210

Acknowledgements

First and foremost, I would like to thank my supervisor Michael Fritz for the organization and work of the PeCaBeau2021 project, for his support in writing this thesis and mentoring. I am very grateful for the opportunity to have written my master's thesis about such an important and interesting topic at AWI. I would also like to thank Peter Kühn for his great insight into the science of the arctic and his support from Tübingen. Moreover, I want to thank Hugues Lantuit for giving me the opportunity to write my master's thesis in his working group with a very familiar atmosphere and for the many opportunities for networking. I am very thankful to the expedition team of PeCaBeau2021 for the preparation of my data and the field work. Also, I would like to thank the lab technicians, especially Justin Lindemann, Birgit Plessen, Sylvia Pinkerneil and Sabine Flaiz, for their patience and help as well as the whole AWI team. Special thanks to Pia Petzold, Leena-Kaisa Viitanen and Justus Gimsa for the support during the last year and the great time in the COPER office.

Finally, I would like to thank my family and friends for always being there for me and the endless support and love.

Declaration of Authorship

I hereby confirm that this thesis has been composed by me and is based on my own work, unless stated otherwise. No other person's work has been used without due acknowledgement in this thesis. All statements taken literally from other writings or referred to by analogy are marked. The submitted work was neither complete nor in essential parts the subject of another examination procedure.

Tübingen, 10.03.2023

Place, Date

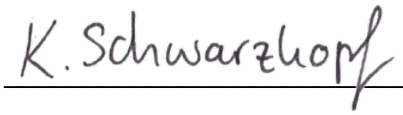

Signature